Self-assembled viologens on HOPG: Solid-state NMR and AFM unravel the location or the anions

Jean Joseph, [a] Frank Palmino,[b] Judicaël Jeannoutot,[b] Mathilde Berville,[a] Jésus Raya,[a] Jean Weiss,[a] Frédéric Chérioux*[b] and Jennifer A. Wytko*[a]

Table of Contents

Experimental methods

Synthesis

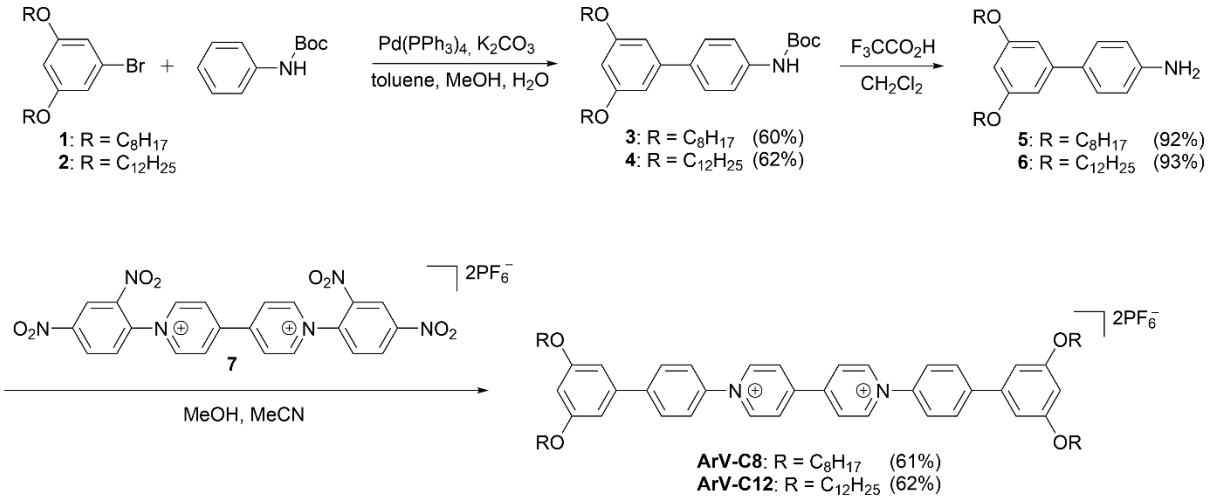

Scheme S1. Synthesis of viologens **ArV-C8** and **ArV-C12**.

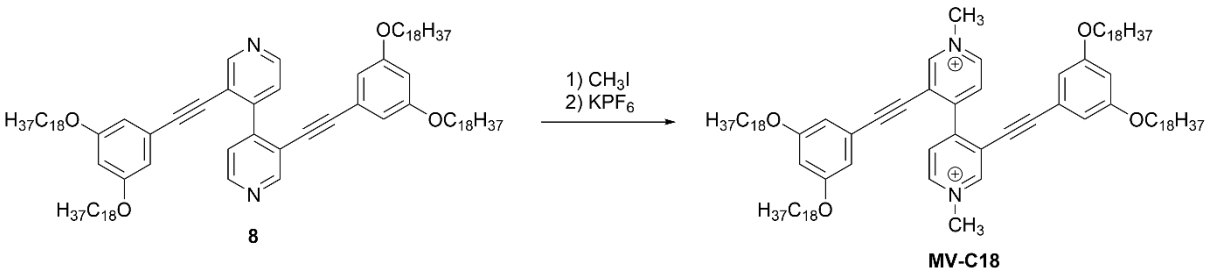

Scheme S2. Synthesis of viologen **MV-C18**.

General synthetic methods. Compounds **ArV-C8** and **ArV-C12** were prepared according to Scheme S1. Compounds **MV-C18** was prepared as shown in Scheme S2. Compounds **1**,[1] **2**,[2] 1,1'-bis(2,4-dinitrophenyl)-4,4'-bipyridinium bis-hexafluorophosphate[3] (**7**), and **8**[4] were prepared by reported methods. Reagents and solvents of reagent-grade were purchased and used without further purification. Evaporation and concentration *in vacuo* were carried out at H_2O-aspirator pressure. Column chromatography was performed with silica gel from Merck (Kieselgel 60; 40-63 µm). Mass spectra were performed by le Service de Spectrométrie de Masse de la Fédération de Chimie LeBel FR2010. Elemental analyses were performed by le Service d'Analyse Elémentaire de la Fédération de

[1] L. A. Tatum, C. J. Jpnson, A. A. P. Fernando, B. C. Ruch, K. K. Barakoti, M. A. Alpuche-Aviles and B. J. King, *Chem. Sci.* 2012, **3**, 3261.

[2] M. Takase, T. Narita, W. Fujita, M. S. Asano, T. Nishinaja, H. Benjen, K. Yoza and K. Müllen, *J. Am. Chem. Soc*. 2013, **135**, 8031.

[3] H. M. Colquhoun, B. W. Burattini, B. W. Greenland, X. Zhu, J. S. Shaw, C. J. Cardin, S. Burrattini, J. M. Eliott, S. Basu, T. B. Gasa and J. F. Stoddart, *Org. Lett*. 2009, **11**, 5239.

[4] Reference 17 in manuscript: J. Richard, J. Joseph, C. Wang, A. Ciesielski, J. Weiss, P. Samorì, V. Mamane and J. A. Wytko*, J. Org. Chem*. 2021, **4**, 3356.

Chimie LeBel FR2010. ^{1}H and ^{13}C NMR spectra were recorded on a Bruker Advance 400 or 500 (400 or 500 MHz) spectrometer. Chemical shifts were determined by taking the solvent as a reference: $CHCl_3$.

UV-visible spectroscopy. All spectra were measured on an Agilent 8453E spectrometer at room temperature in 1, 0.2 or 0.1 cm quartz cells. Solutions were prepared from a stock solution in chloroform at 5 x 10^{-4} M for **ArV-C8** and **ArV-C12** or 1 x 10^{-3} M for **MV-C18**. Each stock solution was sonicated for 1 min before dilutions were carried out. All solutions were measured within one hour of their preparation.

AFM. AFM was used to acquire images in the PeakForce Tapping mode by using an Icon Dimension Bruker microscope. All images were recorded under ambient conditions (air pressure, 298 K) with a resolution of 512 points x 512 lines. The AFM tips used were super-sharp silicon tip, coated with reflective Al having a k = 0.25 $N{\cdot}m^{-1}$ and a tip radius of 2-3 nm (purchased from Bruker). On freshly cleaved HOPG surfaces (also purchased from Bruker), solutions of **ArV-C12** at a concentration of 5 x 10^{-6} $mol{\cdot}L^{-1}$ or **ArV-C8** at a concentration of 1 x 10^{-6} $mol{\cdot}L^{-1}$ in $CHCl_3$ were deposited as 40 µL drops and spin coated at 300 rpm for 30 seconds. The deposition **MV-C18** was performed by drop-casting a solution of $1{\cdot}10^{-6}$ $mol{\cdot}L^{-1}$ in $CHCl_3$. All samples were annealed at 80 °C for 20 min before the AFM measurements were performed to ensure that the solvent had completely evaporated.

Solid-state (ss) MAS NMR. All experiments were performed at room temperature on an AVANCE 500 MHz wide bore spectrometer (BrukerTM) operating at a frequency of 750.12 MHz for ^{1}H, 202.42 MHz for ^{31}P and 188.5 MHz for ^{13}C. All spectra were obtained by spinning samples at 22.5 kHz in a triple resonance $^{1}H/^{31}P/^{13}C$ MAS probe (BrukerTM) designed for 3.2 mm o.d. zirconia rotors closed with vespel caps. For all experiments, including 2D correlations, proton decoupling was obtained using SPINAL-64[5] at a 90 kHz radiofrequency field. To filter out background probe signals and obtain undistorted lineshapes, a speed synchronized spin echo[6] was included inside the experimental pulse sequences in any type of experiment for ^{13}C and ^{31}P (1D or 2D). The corresponding echo-time was set to 88 µs (2 rotation periods).

^{31}P 1D ssNMR. $^{31}P\{^{1}H\}$ DP/MAS spectra (direct polarization) were directly acquired with this pulse scheme[6] and the following conditions: 2.5 µs and 5.5 µs for $P_{90°}$ and $P_{180°}$ pulses, a spectral width of 100 kHz (494.0875 ppm) with 16384 time domain data points (spectral resolution = 12.207 Hz/pt) and 64 scans were added separated by a 30 s recycle delay. This recycling delay was chosen after measuring the T1s by the inversion recovery method[7] (data not shown) and led to the longer T1 of 4.415 s for the series of samples. Spectra are then quantitative and integrals are reliable.

$^{31}P\{^{1}H\}$ CP/MAS spectra were acquired according to the APHH scheme[8] (adiabatic passage through the Hartmann-Hahn conditions). The ^{1}H RF field was swept from 86 to 106 kHz through the Hartmann-Hahn n = 1 condition (96 kHz for ^{1}H, 73.5 kHz for ^{31}P) using the tangential time dependence defined by the shape angle Φ = a tcp/2 where a is the rate of angular dependence. Φ and tcp (contact time) were set to 88° and 3 ms after optimization.[9] For the shorter contact times like those used inside the ^{1}H to ^{31}P short-range correlations, no APHH scheme was used because it is less efficient[9] than classical rectangular pulse shapes. In these cases (p15 = 150 µs) the field strengths were kept constant for both nuclei (96 kHz for ^{1}H, 73.5 kHz for ^{31}P). CP/MAS spectra were acquired with the same spectral parameters as above (100 kHz spectral width, 16384 time domain data points, spectral resolution = 12.207 Hz/pt). Recycling time was set to 3 s and 32 scans were added, leading to equal or higher peaks intensity than for DP/MAS. Raw data were processed with a 10 Hz Lorentzian filter followed by Fourier

[5] B. M. Fung, A. K. Khitrin, and K. J. Ermolaev*, J. Magn. Reson*. 2000, **142**, 97.
[6] E. L. Hahn, *Phys. Rev.* 1950, **80**, 580.
[7] K. A. Christensen, D. M. Grant, E. M. Schulman and C. Walling, *J. Phys. Chem.* 1974, **78**, 1971.
[8] S. Hediger, B. H. Meier, N. D. Kurur, G. Bodenhausen and R. R. Ernst, *Chem. Phys. Lett.* 1994, **223**, 283.
[9] J. Raya, B. Perrone and J. Hirschinger, *J. Magn. Reson.* 2013, **227**, 93.

transformation without zero filling. Chemical shifts are given respective to PO_4 using H_3PO_4 (80% in D_2O) as a secondary reference**.**

^{13}C 1D ssNMR. Similarly, $^{13}C\{^1H\}$ CP/MAS spectra were acquired with the same pulse scheme (APHH[8]) with similar parameters; the ^1H RF field was swept from 71.7 to 91.7 kHz through the Hartmann-Hahn n = 1 condition (81.7 kHz for ^1H, 59.2 kHz for ^{13}C) for the long contact-time cases (tcp = 2 ms). Again, for short contact-times (45 µs), the regular rectangular pulse scheme was preferred (1D or 2D). All ^{13}C spectra were obtained with the following conditions: 50 kHz spectral width (397.6148 ppm), 2048 time domain data points (24.414 Hz/pt), 2048 scans and 3 s recycling delay. A 100 Hz Lorentzian filter was applied prior to Fourier transform over 4096 points (zero filling by 2048 points). Chemical shifts are given with respect to tetramethysilane (TMS) using adamantane as a secondary reference.[10]

^{31}P and ^{13}C 2D ssNMR. To decipher the structure of our supramolecular assemblies, a series of 2D ^1H-^{13}C HETCOR with FSLG (Frequency Shifted Lee-Goldburg)[11] irradiation during the evolution time[11] were conducted using both ^{13}C and ^{31}P. Based on the nature of the dipolar interactions, which occur through space, these bidimensional experiments allow detection of spatial proximities between the nuclei under investigation, namely ^1H with ^{13}C and ^1H with ^{31}P. Moreover, tuning contact times from short (ca 45 µs) to longer times (ca 250 µs or more) allows assignment of ^1H and ^{13}C peaks because the shortest times indicate which proton is directly connected to which carbon and which are remotely spaced. Similarly, for the phosphorus and as coherences are built through space, with short contact times it is possible to determine which of the previously assigned protons are closest to the phosphorus and therefore to know where the PF_6^- anions are located within the supramolecular assemblies. For this purpose, a series of bidimensional ^1H-^{13}C and ^1H-^{31}P FSLG HETCOR were run keeping the exact same parameters for the proton (same homonuclear decoupling effective field, same frequency offset, same t1 increments); the duration of the successive FSLG pulses was 6.667 µs (32.4328 ppm ^1H spectral width and 150 kHz effective ^1H-^1H decoupling field) and the magic-angle pulse length was 1.3 µs. A total of 128 complex data points were acquired in the ^1H indirect dimension and for each t1 increment, 2048 scans were accumulated leading to a time resolution of 3.9462 ms (253.4057 Hz) for ^1H. The ^1H-X FSLG HETCOR experiment consists in taking a succession of 1D ^1H-X CP/MAS spectra where the proton has previously experienced an incremented time evolution with homonuclear decoupling; thus, the direct dimension parameters for ^{13}C and ^{31}P were kept the same as the previously decribed for 1D $^{13}C\{1H\}$ CP/MAS and $^{31}P\{1H\}$ CP/MAS. Prior to Fourier transformation, a Lorentzian line broadening of 25 Hz was applied in the direct dimension for ^{31}P and 12 Hz for ^{13}C and the proton dimension apodization was performed with a 90° shifted squared sine-bell function.

[10] C. R. Morcombe and K. W. Zilm, *J. Magn. Reson*. 2003, **162**, 479.
[11] B.-J. van Rossum, H. Förster and H. J. M. de Groot, *J. Magn. Reson*. 1997, **124**, 516.

Synthetic methods

Compound 3. Tetrakis(triphenylphosphine)palladium (0.42 g, 0.3 mmol) was added to a degassed solution of 4-(*N*-Boc-amino)phenylboronic acid (1.72 g, 7.3 mmol), potassium carbonate (4.02 g, 29.1 mmol) and compound **1** (1.50 g, 3.6 mmol) in a mixture of toluene/methanol/water (200/30/18 mL). The mixture was refluxed under argon for 48 h. After cooling to r.t., the mixture was decanted. The organic layer was washed with an aqueous solution of 2 M Na_2CO_3 (100 mL), and twice with water. The organic layer was dried over Na_2SO_4 and concentrated. The crude material was purified by column chromatography (SiO_2, pentane/AcOEt (9/1)). The fractions containing the product were concentrated, and then pentane (12 mL) and acetonitrile (4 mL) were added to the residue. The upper layer was recovered and extracted with acetonitrile (4 mL). This operation was repeated until the upper layer showed only one spot on TLC (SiO_2, pentane/AcOEt (99/1)). The upper layer was concentrated and dried under vacuum to afford compound **3** as a colorless oil (1.15 g, 2.2 mmol, 60%) that was used without further purification for the next step. ^{1}H NMR (500 MHz, $CDCl_3$, 25 °C) δ = 0.89 (t, J = 7.0 Hz, 6H), 1.29 (m, 16H), 1.46 (tt, J = 7.0 Hz, J = 7.4 Hz, 4H), 1.53 (s, 9H), 1.79 (tt, J = 7.4 Hz, J = 6.6 Hz, 4H), 3.98 (t, J = 6.6 Hz, 4H), 6.42 (t, J = 2.2 Hz, 1H), 6.50 (br. s, 1H), 6.67 (d, J = 2.2 Hz, 2H), 7.40 (d, J = 8.6 Hz, 2H), 7.50 (d, J = 8.6 Hz, 2H). ^{13}C NMR (125 MHz, $CDCl_3$, 25 °C) δ = 14.3, 22.9, 26.3, 28.6, 29.47, 29.52, 29.6, 32.0, 68.3, 80.9, 100.0, 105.7, 118.8, 127.9, 136.2, 138.0, 142.9, 152.9, 160.8. ESI HRMS: *m/z* = 526.3929 ($[M+H]^+$).

Compound 4. Tetrakis(triphenylphosphine)palladium (0.32 g, 0.3 mmol) was added to a degassed solution of 4-(N-Boc-amino)phenylboronic acid (1.35 g, 5.7 mmol), potassium carbonate (3.15 g, 22.8 mmol) and compound **2** (1.50 g, 2.9 mmol) in a mixture of toluene/methanol/water (100/30/18 mL). The mixture was refluxed under argon for 48 h. After cooling to r.t., the mixture was decanted. The organic layer was washed with 2 M $Na_2CO_{3(aq)}$ (100 mL), and twice with water. The organic layer was dried over Na_2SO_4 and concentrated. The crude material was purified by column chromatography (SiO_2, pentane/AcOEt (9/1)). The fractions containing the product were concentrated. Pentane (12 mL) and acetonitrile (4 mL) were added to the residue. The upper layer was recovered and extracted with acetonitrile (4 mL). This operation was repeated until the upper layer showed only one spot on TLC (SiO_2, pentane/AcOEt (99/1)). The upper layer was concentrated and dried under vacuum to afford compound **4** as a colorless oil (1.14 g, 1.8 mmol, 62%). ^{1}H NMR (500 MHz, $CDCl_3$, 25 °C) δ = 0.86 (t, J = 6.9 Hz, 6H), 1.26 (m, 32H), 1.46 (tt, J = 7.2 Hz, J = 7.5 Hz, 4H), 1.52 (s, 9H), 1.78 (tt, J = 7.5 Hz, J = 6.6 Hz, 4H), 3.98 (t, J = 6.6 Hz, 4H), 6.42 (t, J = 2.2 Hz, 1H), 6.50 (br. s, 1H), 6.67 (d, J = 2.2 Hz, 2H), 7.41 (d, J = 8.2 Hz, 2H), 7.50 (d, J = 8.2 Hz, 2H). ^{13}C NMR (125 MHz, $CDCl_3$, 25 °C) δ = 14.4, 22.9, 26.3, 28.6, 29.5, 29.58, 29.63, 29.80, 29.83, 29.86, 29.89, 31.1, 68.3, 80.9, 100.0, 105.7, 118.8, 127.9, 136.2, 137.0, 142.9, 152.9, 160.8. ESI HRMS: Calc. *m/z* = 638.5241 ($[M+H]^+$).

Compound 5. Trifluoroacetic acid (2 mL, 26.1 mmol) was added dropwise to a solution of compound **3** (1.07 g, 2.0 mmol) in dichloromethane (75 mL) under argon at 0 °C. The solution was allowed to warm slowly to r.t. and was stirred for 38 h. The solution was poured into a saturated aqueous solution of Na_2CO_3 (100 mL). The organic layer was washed twice with water, dried over Na_2SO_4, filtered and solvent was evaporated under vacuum. The crude material was purified by column chromatography (SiO_2, cyclohexane/AcOEt (1/1)) to afford compound **5** as a pale pink oil (0.80 g, 1.9 mmol, 92%). ^{1}H NMR (500 MHz, $CDCl_3$, 25 °C) δ = 0.89 (t, J = 6.9 Hz, 6H), 1.26 (m, 20H), 1.79 (tt, J = 7.4 Hz, J = 6.7 Hz, 4H), 3.70 (br. s, 2H), 3.98 (t, J = 6.7 Hz, 4H), 6.39 (t, J = 2.2 Hz, 1H), 6.66 (d, J = 2.2 Hz, 2H), 6.75 (d, J = 8.4 Hz, 2H), 7.38 (d, J = 8.4 Hz, 2H). ^{13}C NMR (125 MHz, $CDCl_3$, 25 °C) δ = 14.3, 22.9, 26.3, 27.1, 29.5, 29.6, 32.0, 68.3, 99.5, 105.4, 115.4, 128.2, 131.8, 143.4, 146.2, 160.7. ESI HRMS: *m/z* = 426.3317 ($[M+H]^{+)}$

Compound 6. Trifluoroacetic acid (2 mL, 26.1 mmol) was added dropwise to a solution of compound **4** (1.10 g, 1.7 mmol) in dichloromethane (75 mL) under argon at 0 °C. The solution was allowed to warm slowly to r.t. and was stirred for 38 h. The solution was poured into a saturated aqueous solution of

Na_2CO_3 (100 mL). The organic layer was washed twice with water, dried over Na_2SO_4, filtered and solvent was removed under vacuum. The crude material was purified by column chromatography (SiO_2, cyclohexane/AcOEt (4/1)) to afford compound **6** as a colorless oil (0.92 g, 1.7 mmol, 93%). ^{1}H NMR (500 MHz, $CDCl_3$, 25 °C) δ = 0.88 (t, J = 6.8 Hz, 6H), 1.26 (m, 36H), 1.77 (tt, J = 7.4 Hz, J = 6.6 Hz, 4H), 3.72 (br. s, 2H), 3.98 (t, J = 6.6 Hz, 4H), 6.39 (t, J = 2.0 Hz, 1H), 6.66 (d, J = 2.0 Hz, 2H), 6.71 (d, J = 8.4 Hz, 2H), 7.38 (d, J = 8.4 Hz, 2H). ^{13}C NMR (125 MHz, $CDCl_3$, 25 °C) δ = 14.4, 22.9, 26.3, 27.1, 29.54, 29.58, 29.63, 29.82, 29.86 29.9, 32.1, 68.3, 99.5, 105.4, 115.4, 128.2, 131.8, 143.4, 146.2, 160.7. ESI HRMS: *m/z* = 538.4681 ($[M+H]^+$).

Compound ArV-C8 . Compound **5** (0.79 g, 1.9 mmol) was added to a solution of 1,1'-bis(2,4-dinitrophenyl)-4,4'-bipyridinium bis-hexafluorophosphate[3] (**7**) (0.65 g, 0.8 mmol) in a mixture of MeCN/EtOH (100 mL, 1/1). The resulting turned dark brown solution was refluxed for 16 h under argon. After cooling to r.t., solvents were removed under vacuum. The crude material was dissolved in hot dichloromethane and methanol was added. The resulting precipitate was filtered. The solid was dried under vacuum to afford compound **ArV-C8** as a pale yellow solid (0.655 g, 0.5 mmol, 61%). m.p. dec. 236 °C. E.A. (%) calcd for $C_{66}H_{90}N_2O_4P_2F_{12}$ (1264.62): C 62.65, H 7.17, N 2.21; found: C 62.67, H 6.92, N 2.35. ^{1}H NMR (500 MHz, $CDCl_3$, 25 °C, 1.5 x 10^{-3} M) δ = 0.88 (t, J = 6.8 Hz, 12H), 1.28-1.33 (m, 32H), 1.43 (m, 8H), 1.77 (quin, J = 7.5 Hz, 8H), 3.93 (t, J = 6.5 Hz, 8H), 6.47 (t, J = 2.0 Hz, 2H), 6.63 (d, J = 2.0 Hz, 4H), 7.67 (d, J = 7.9 Hz, 4H), 7.74 (d, J = 7.9 Hz, 4H), 8.45 (d, J = 4.6 Hz, 4H), 8.90 (d, J = 4.6 Hz, 4H). ^{13}C NMR (125 MHz, $CDCl_3$, 25 °C, 1.5x10^{-3} M) δ = 14.3, 22.8, 26.2, 29.42, 29.43, 29.6, 32.0, 68.4, 101.6, 106.0, 124.4, 128.1, 129.5, 140.1, 141.2, 144.7, 145.4, 151.5, 161.0. ^{31}P NMR (121 MHz, $CDCl_3$) δ -144.84 (quin, J = 714 Hz). ^{19}F NMR (282 MHz, $CDCl_3$) δ -71.96 (d, J = 150 Hz). ESI HRMS: *m/z* = 487.3385 ($[M]^{2+}$). UV-visible (1 x 10^{-5} M in $CHCl_3$) λ (nm) (ε (M^{-1} cm^{-1}): 263 (36200), 392 (11000).

Compound ArV-C12. Compound **6** (0.89 g, 1.7 mmol) was added to a solution of 1,1'-bis(2,4-dinitrophenyl)-4,4'-bipyridinium bis-hexafluorophosphate[3] (**7**) (0.57 g, 0.8 mmol) in a mixture of MeCN/EtOH (100 mL, 1/1). The solution turned dark brown. The solution was refluxed for 16 h under argon. After cooling to r.t., solvents were removed under vacuum. The crude material was dissolved in hot dichloromethane and methanol was added. The resulting precipitate was filtered. The solid was dried under vacuum to afford compound **ArV-C12** as a pale yellow solid (0.726 g, 0.5 mmol, 62%). m.p. turns orange at 190 °C, then dec. 230 °C. E. A. (%) calcd for $C_{82}H_{122}N_2O_4P_2F_{12}$ (1488.87): C 66.11, H 8.25, N 1.88; found: C 66.09, H 7.84, N 2.04. ^{1}H NMR (500 MHz, $CDCl_3$, 25 °C, 2.5 x 10^{-3} M) δ = 0.87 (t, J = 6.9 Hz, 12H), 1.26-1.33 (m, 48H), 1.45 (tt, J = 7.5 Hz, J = 7.1 Hz, 8H), 1.77 (tt, J = 7.5 Hz, J = 6.3 Hz, 8H), 3.93 (t, J = 6.3 Hz, 8H), 6.47 (t, J = 2.0 Hz, 2H), 6.63 (d, J = 2.0 Hz, 4H), 7.68 (d, J = 8.3 Hz, 4H), 7.75 (d, J = 8.3 Hz, 4H), 8.46 (d, J = 6.1 Hz, 4H), 8.90 (d, J = 6.1 Hz, 4H). ^{13}C NMR (125 MHz, $CDCl_3$, 25 °C, 2.5 x 10^{-3} M) δ = 14.3, 22.9, 26.2, 29.46, 29.5, 29.6, 29.79, 29.82, 29.9, 32.1, 68.4, 101.6, 105.9, 124.4, 128.1, 129.5, 140.1, 141.2, 144.7, 145.4, 151.5, 161.0. ^{31}P NMR (121 MHz, $CDCl_3$) δ -144.73 (sept, J = 712 Hz). ^{19}F NMR (282 MHz, $CDCl_3$) δ -71.76 (d, J = 712 Hz). ESI HRMS: *m/z* = 599.4614 ($[M]^{2+}$). UV-visible (7.8 x 10^{-6} M in $CHCl_3$) λ (nm) (ε (M^{-1} cm^{-1}): 263 (36700), 392 (13300).

Compound MV-C18. A solution of **8**[4] (200 mg, 0.14 mmol) in iodomethane (5 mL) was refluxed under argon overnight. After cooling to rt, the iodomethane was then removed by trap to trap vacuum and the resulting red residue dissolved in a minimal amount of MeCN. A saturated aqueous solution of KPF_6 was added and a brown solid precipitated. The solid was filtered, washed with water and dried to afford viologen **MV-C18** as an orange powder (245 mg, 0.14 mmol, quantitative). E.A. (%) calcd for $C_{100}H_{166}F_{12}N_2O_4P_2$: C, 68.62; H, 9.56; N, 1.60; found: C, 68.73; H, 9.62; N, 1.54. ^{1}H NMR (400 MHz, $CDCl_3$) δ 0.88 (t, J = 6.8 Hz, 12H), 1.10-1.48 (m, 120H), 1.67 (quint, J = 6.8 Hz, 8H), 3.78 (t, J = 6.8 Hz, 8H), 4.32 (s, 6H), 6.43 (s, 2H), 6.50 (s, 4H),7.94 (d, J = 6.4 Hz, 2H), 8.73 (d, J = 6.4 Hz, 2H), 8.83 (s, 2H). ^{13}C NMR (125 MHz, $CDCl_3$) δ 14.3, 22.8, 26.2, 29.3, 29.5, 29.7, 29.83, 29.84, 29.90, 29.92, 29.93, 29.94, 32.1, 49.1, 68.5, 79.9, 103.5, 105.7, 110.1, 121.1, 124.0, 129.1, 144.5, 147.9, 150.9, 160.4. ^{31}P NMR (121 MHz, $CDCl_3$) δ -144.73 (sept, J = 712 Hz). ^{19}F NMR (282 MHz, $CDCl_3$) δ -71.76 (d, J = 712 Hz). ESI HRMS: *m/z* = 729.6446 ($[M]^{2+}$). UV-visible (1 x 10^{-5} M in $CHCl_3$) λ (nm) (ε (M^{-1} cm^{-1}): 303 (24600), 377 (9200).

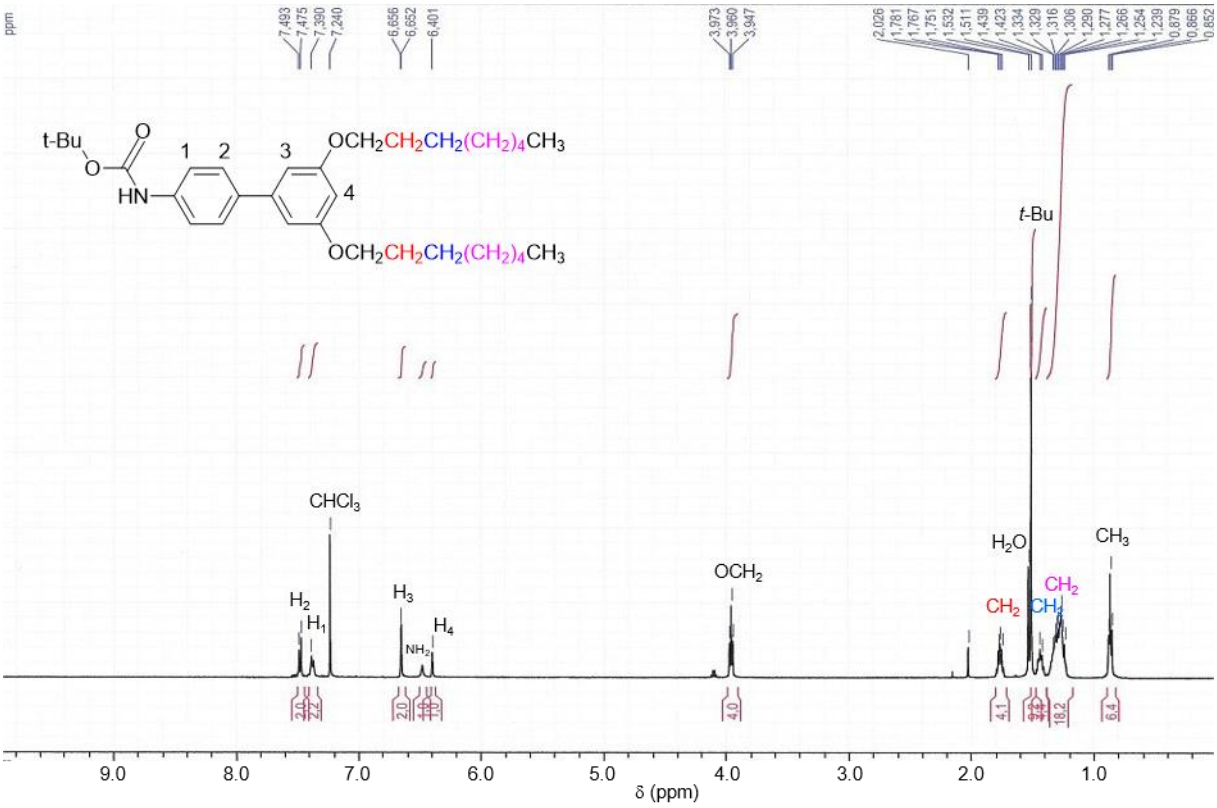

Figure S1. ^{1}H NMR (500 MHz, $CDCl_3$) of compound **3**.

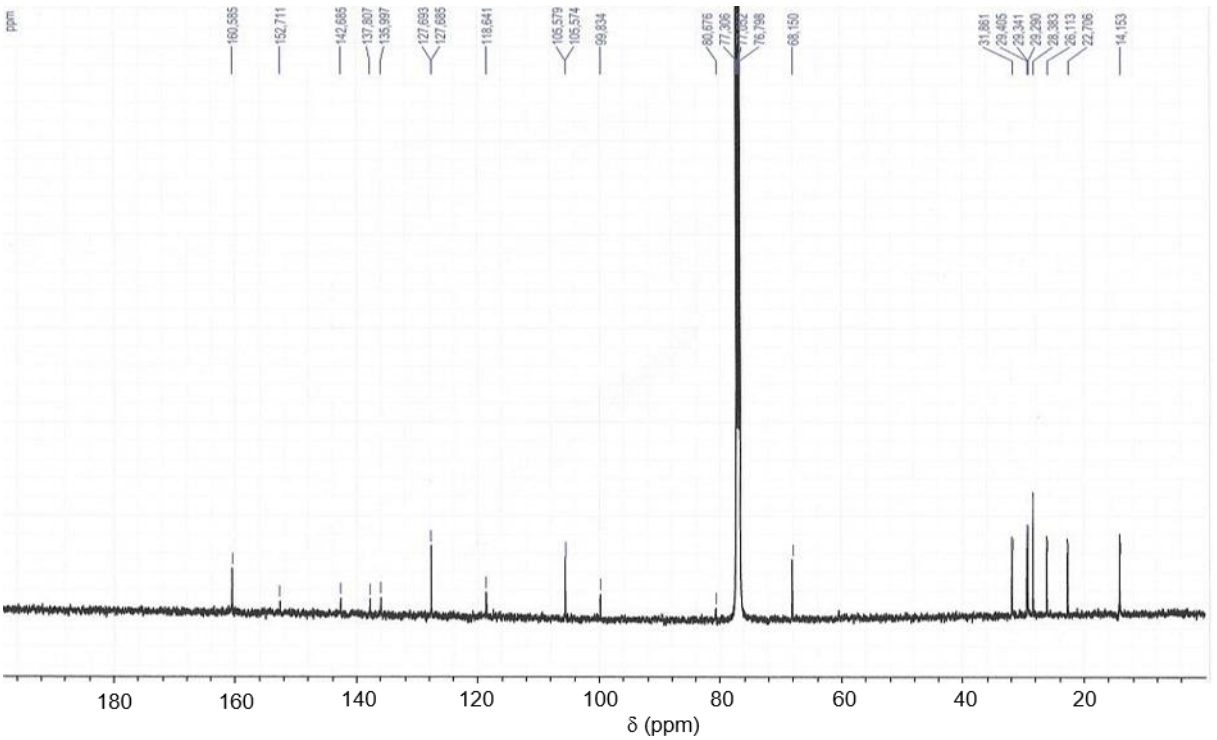

Figure S2. ^{13}C NMR (125 MHz, $CDCl_3$) of compound **3**.

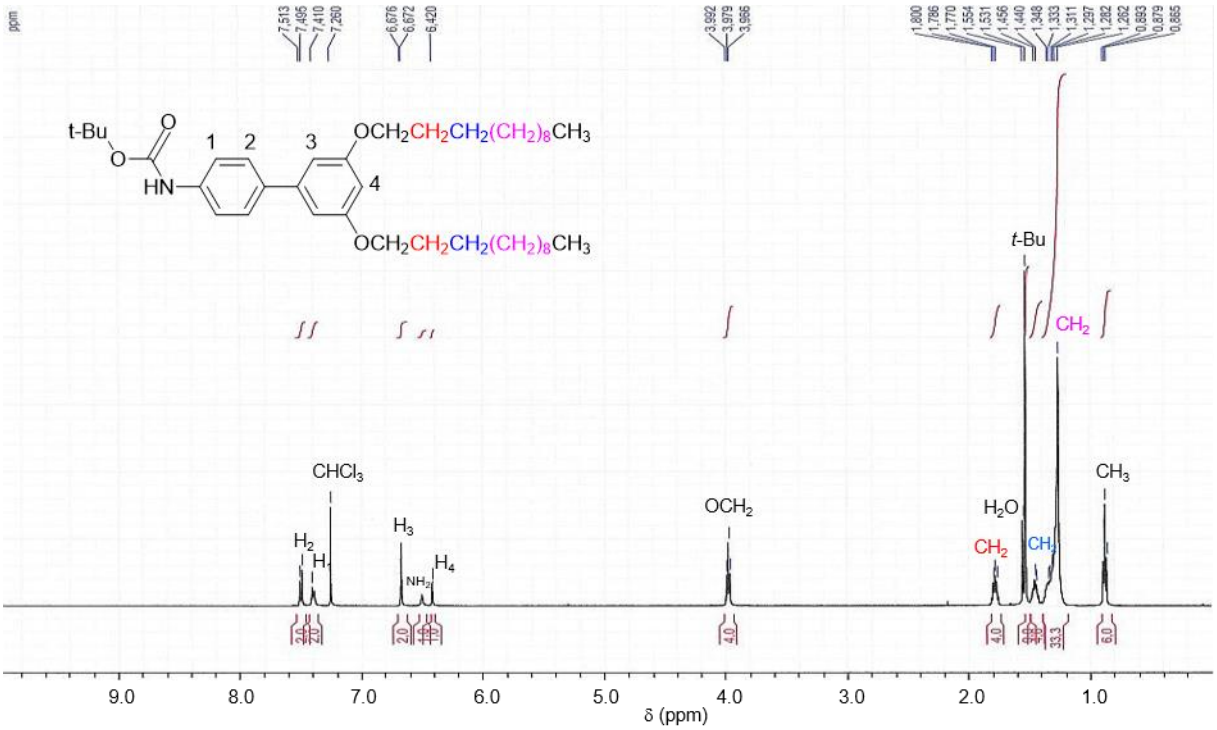

Figure S3. ^{1}H NMR (500 MHz, $CDCl_3$) of compound **4**.

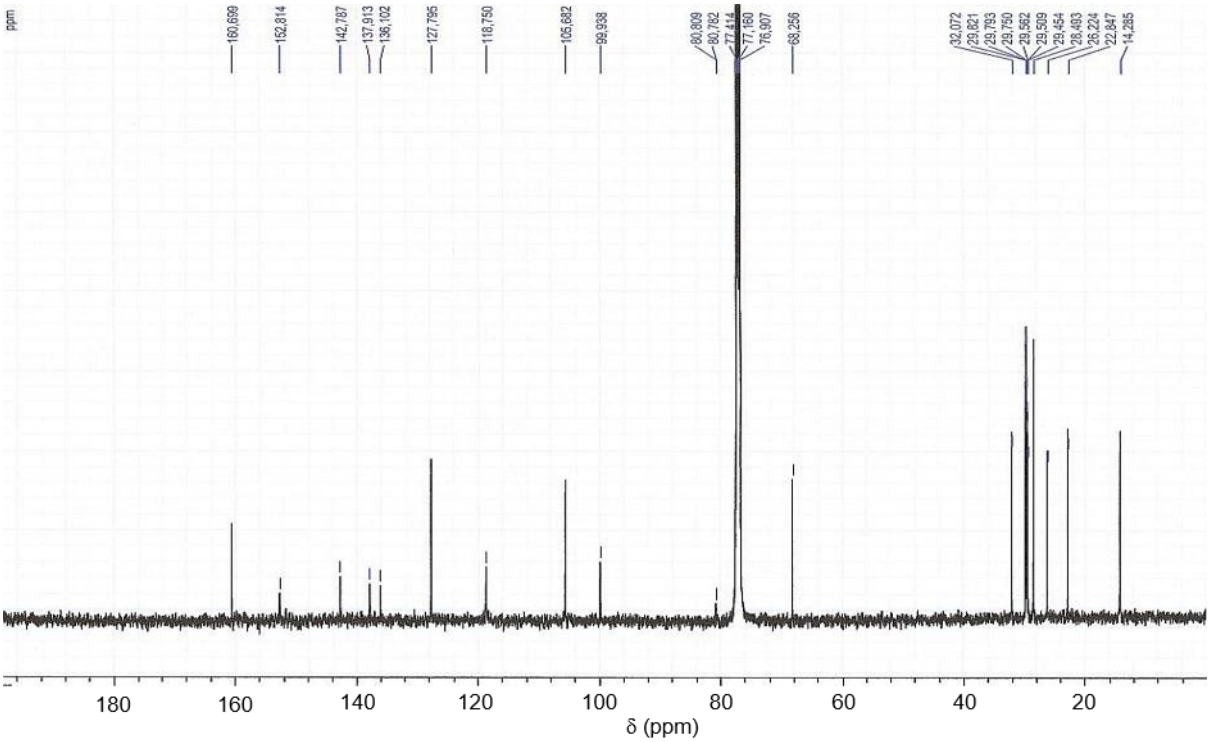

Figure S4. ^{13}C NMR (125 MHz, $CDCl_3$) of compound **4**.

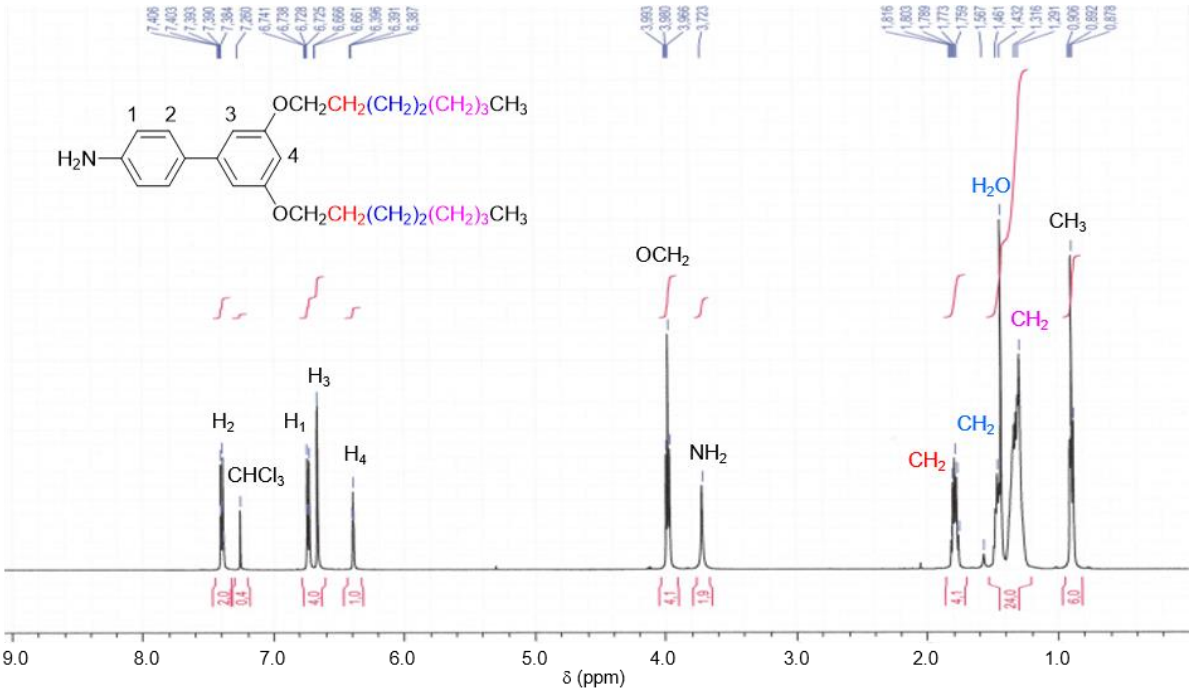

Figure S5. ^{1}H NMR (500 MHz, $CDCl_3$) of compound **5**.

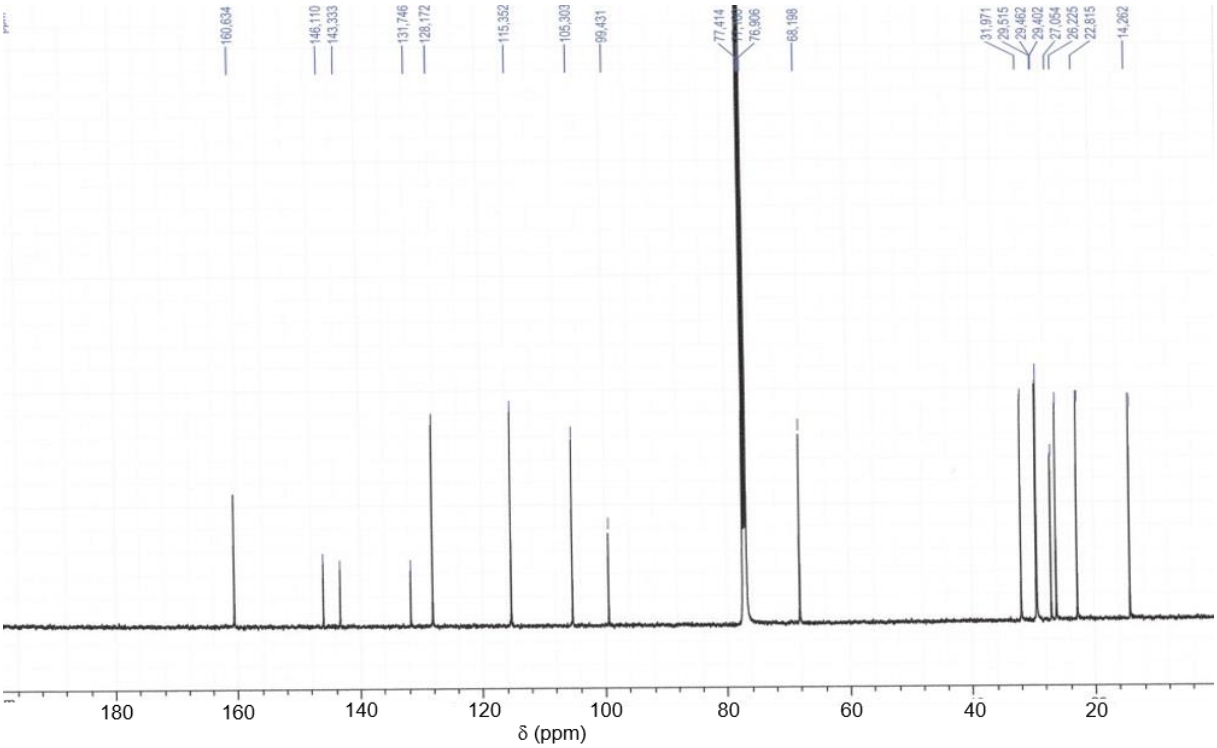

Figure S6. ^{13}C NMR (125 MHz, $CDCl_3$) of compound **5**.

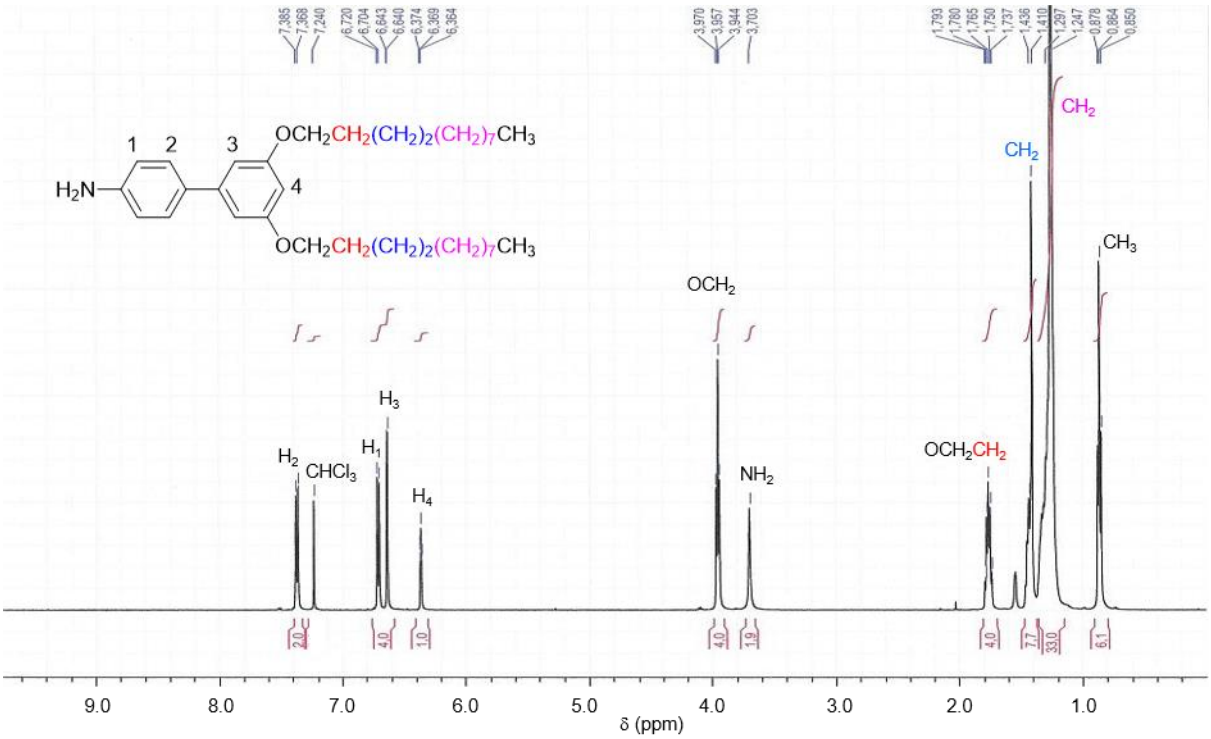

Figure S7. ^{1}H NMR (500 MHz, $CDCl_3$) of compound **6**.

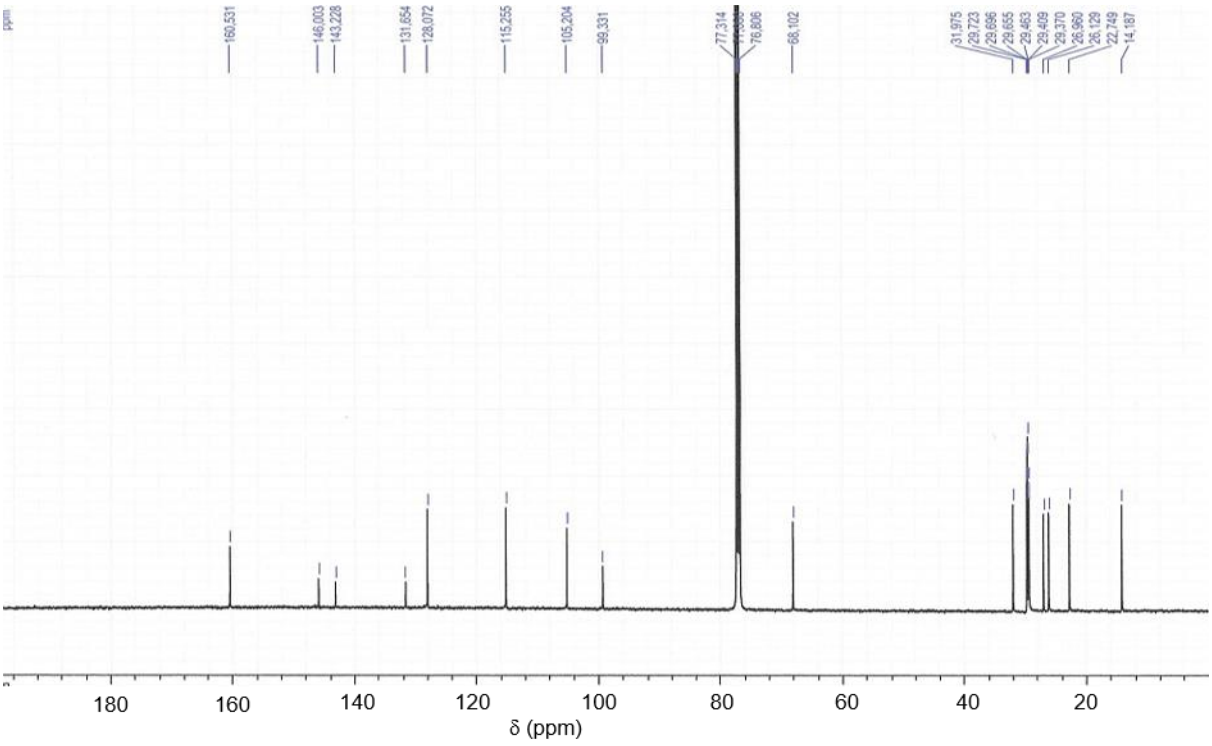

Figure S8. ^{13}C NMR (125 MHz, $CDCl_3$) of compound **6**.

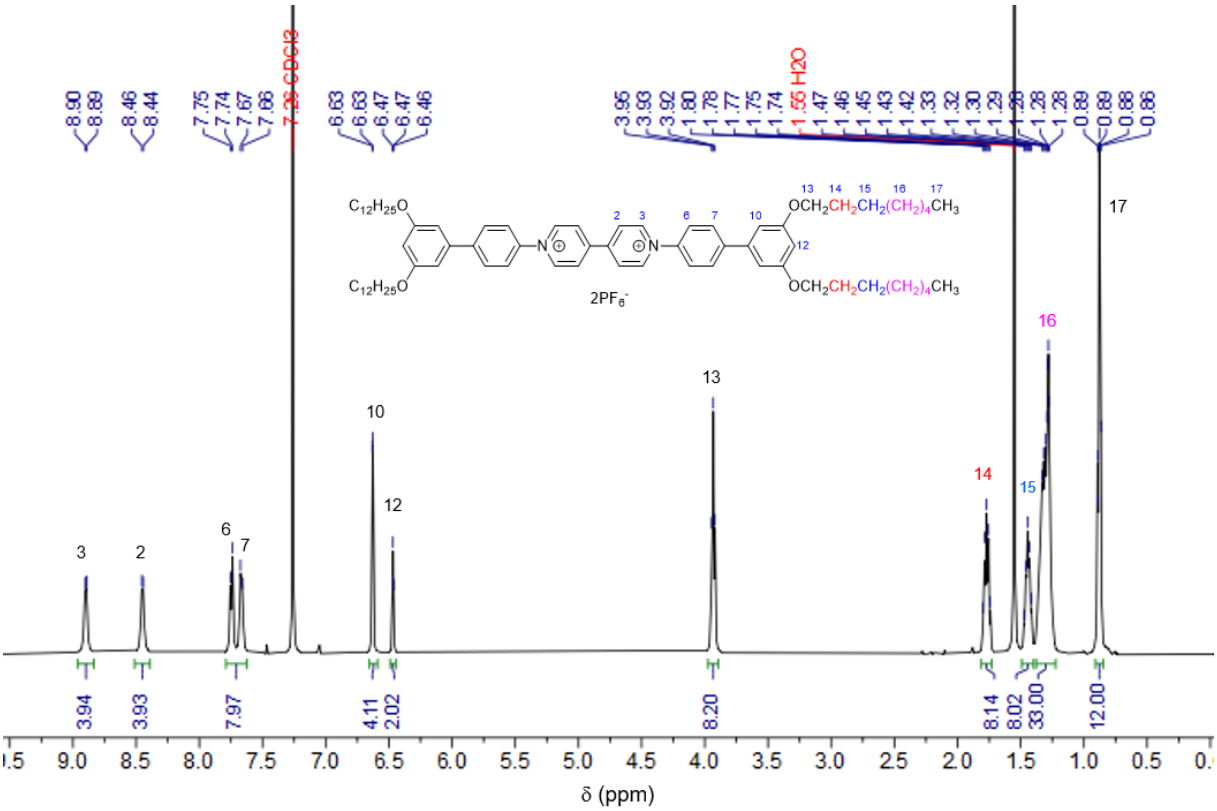

Figure S9. ^{1}H NMR (500 MHz, $CDCl_3$) of viologen **ArV-C8**.

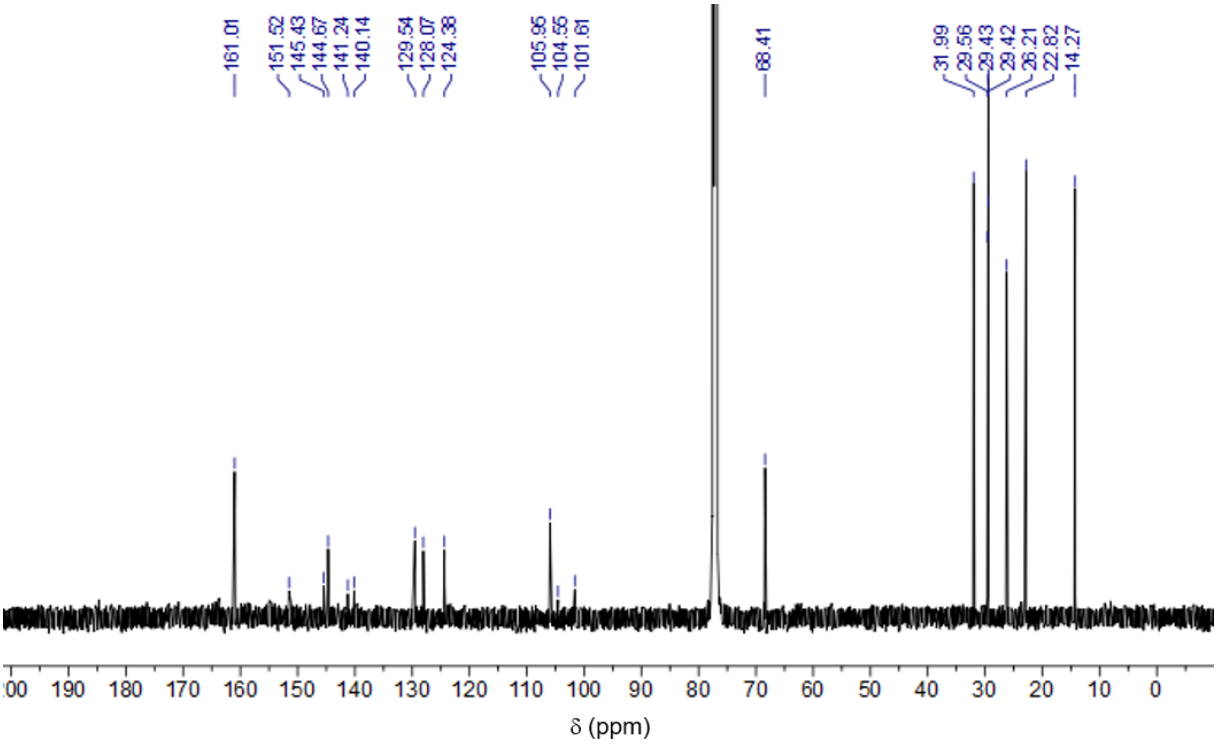

Figure S10. ^{13}C NMR (125 MHz, $CDCl_3$) of viologen **ArV-C8**.

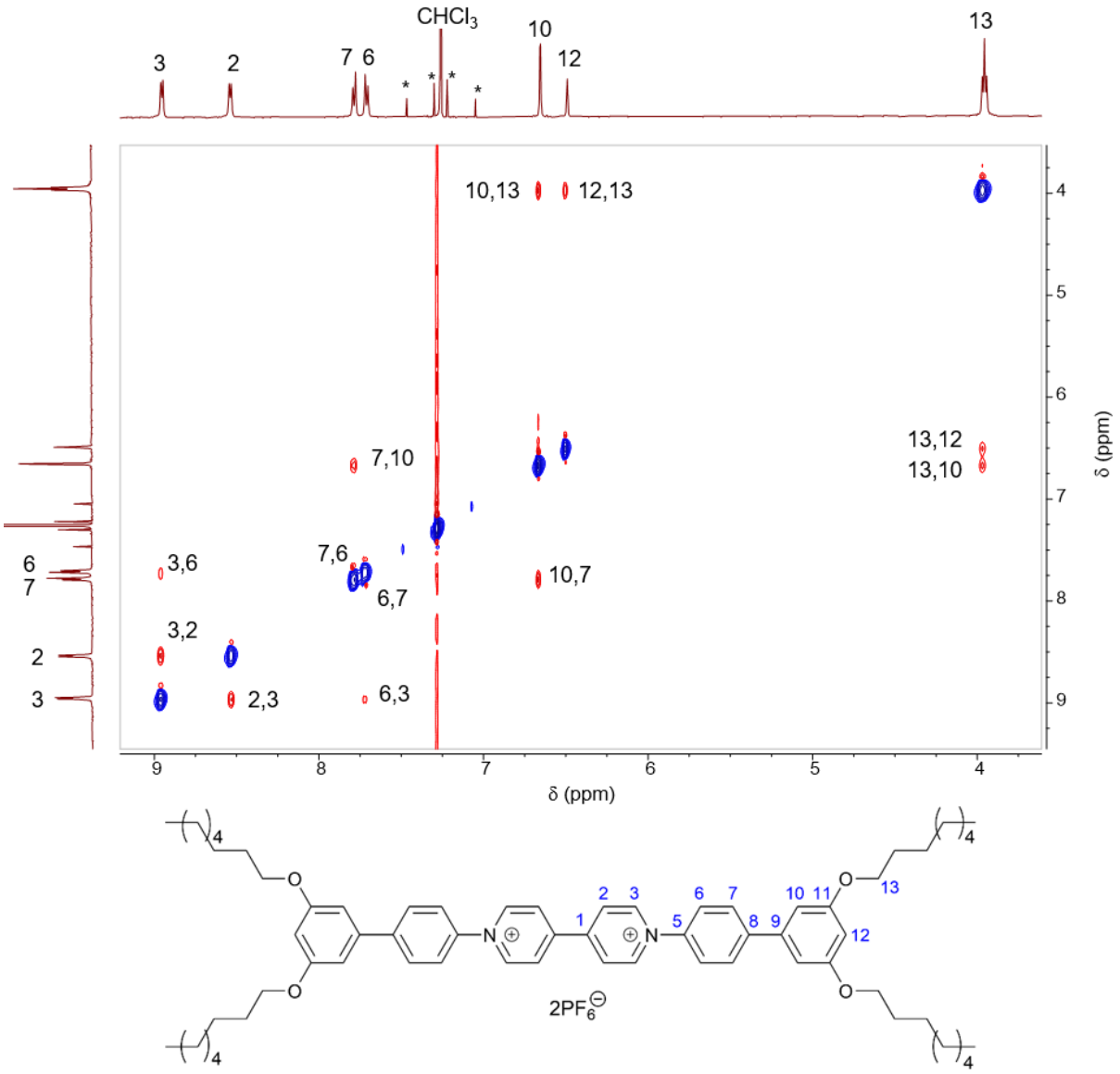

Figure S11. ROESY NMR spectrum (500 MHz, $CDCl_3$) of viologen **ArV-C8**.

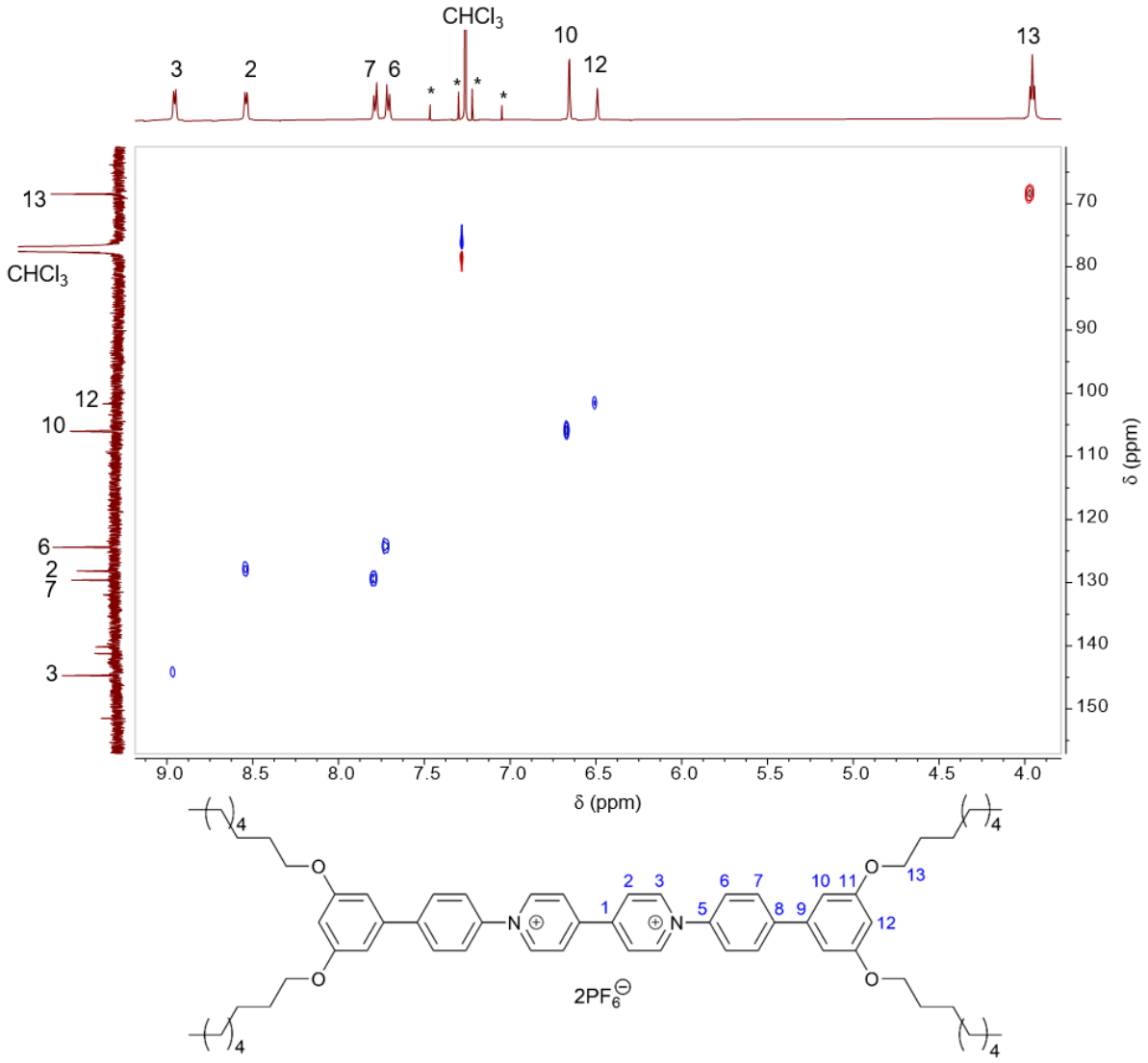

Figure S12. ^{1}H-^{13}C HSQC NMR spectrum (500 MHz, $CDCl_3$) of viologen **ArV-C8**.

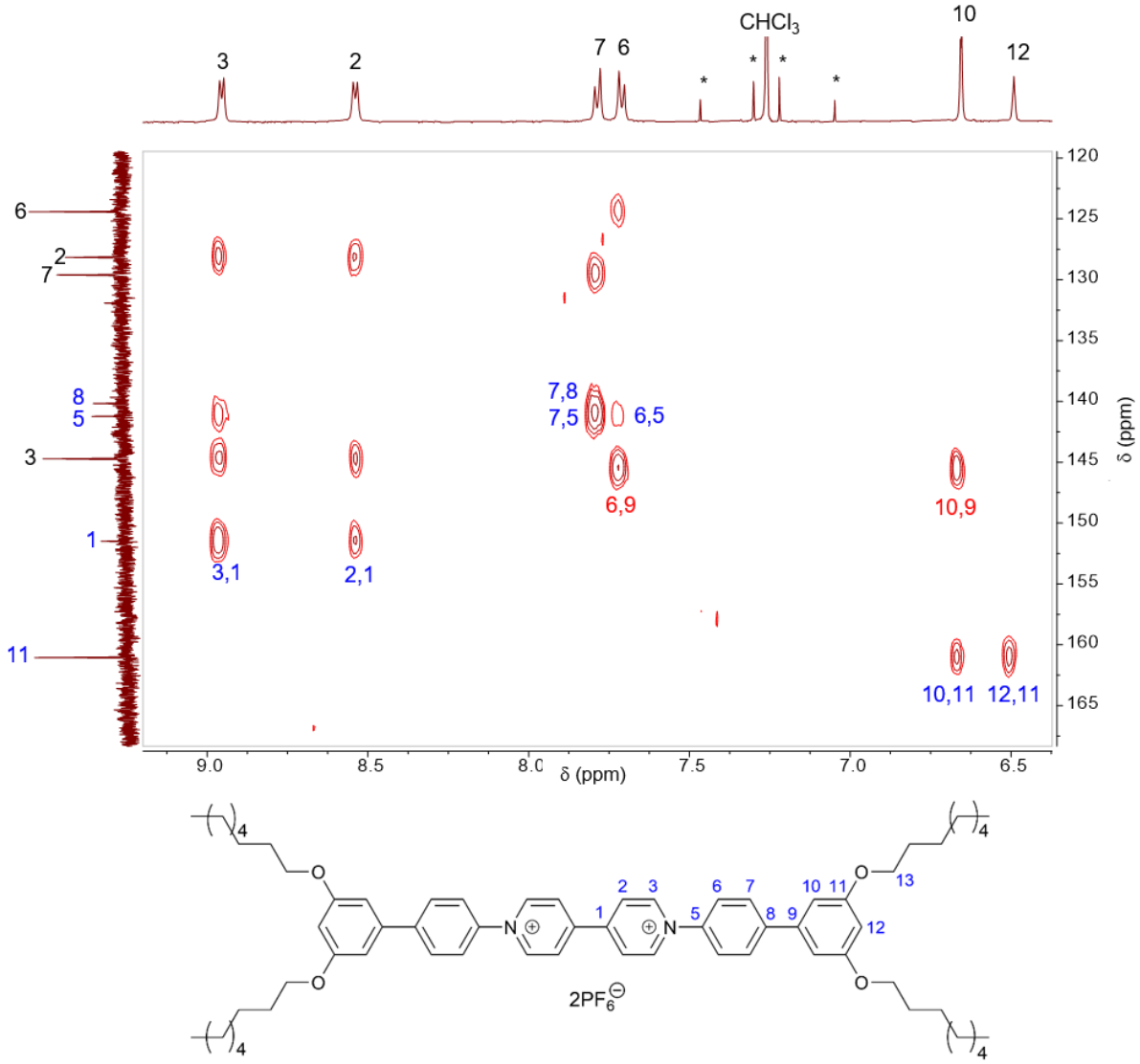

Figure S13. ^{1}H-^{13}C HMBC NMR spectrum (500 MHz, $CDCl_3$) of viologen **ArV-C8**. Attributions in blue and red were determined with this spectrum. The ^{13}C peak for C9 is missing in this spectrum but is visible in Figure S10.

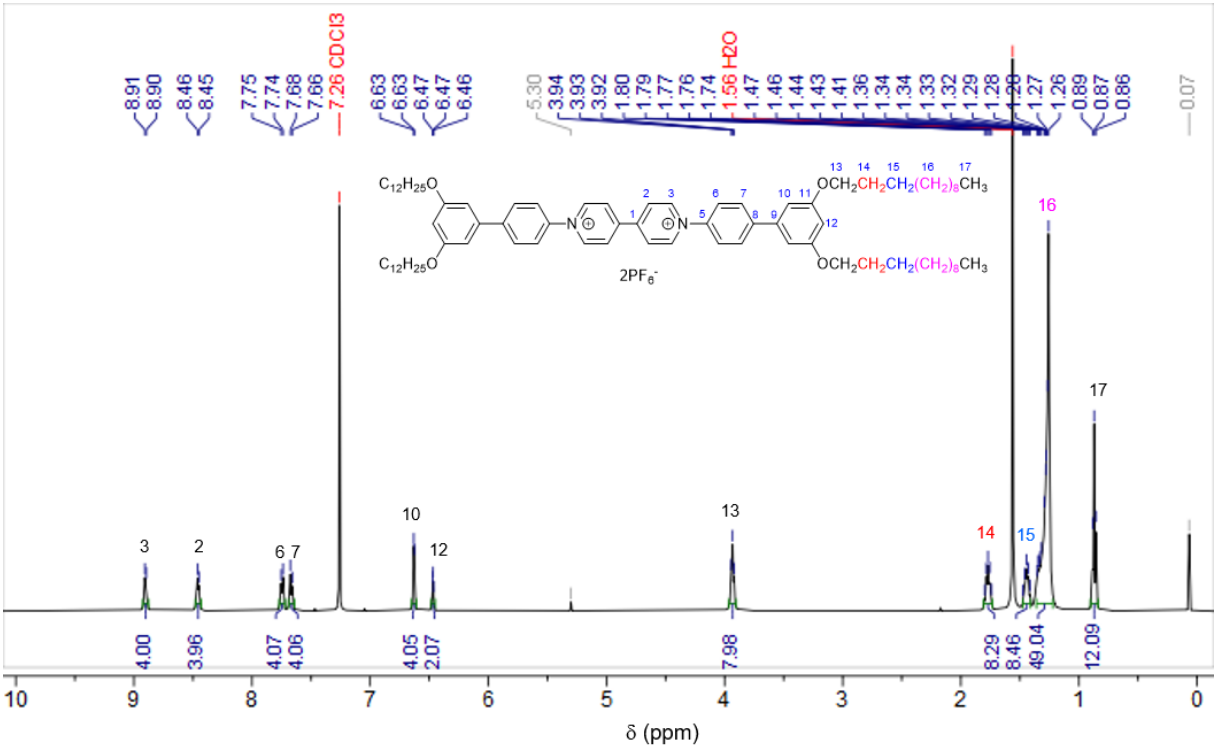

Figure S14. ^{1}H NMR (500 MHz, $CDCl_3$) of viologen **ArV-C12**.

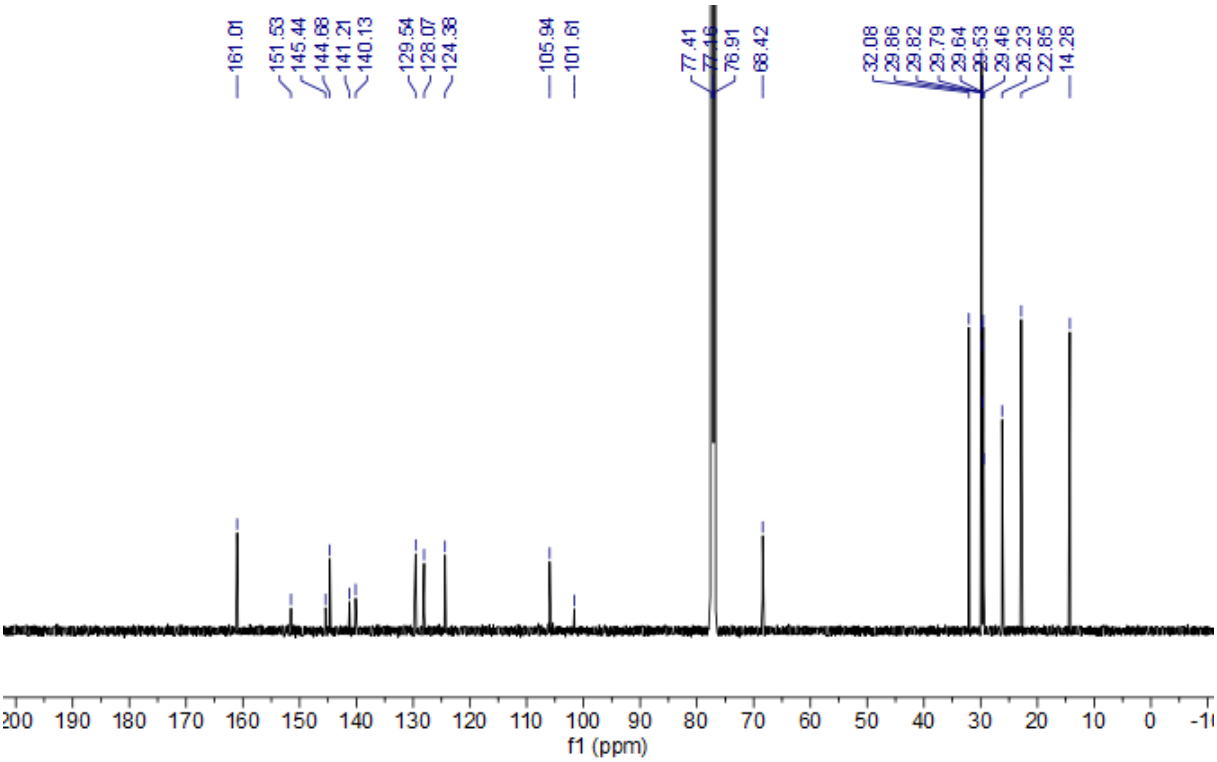

Figure S15. ^{13}C NMR (125 MHz, $CDCl_3$) of viologen **ArV-C12**.

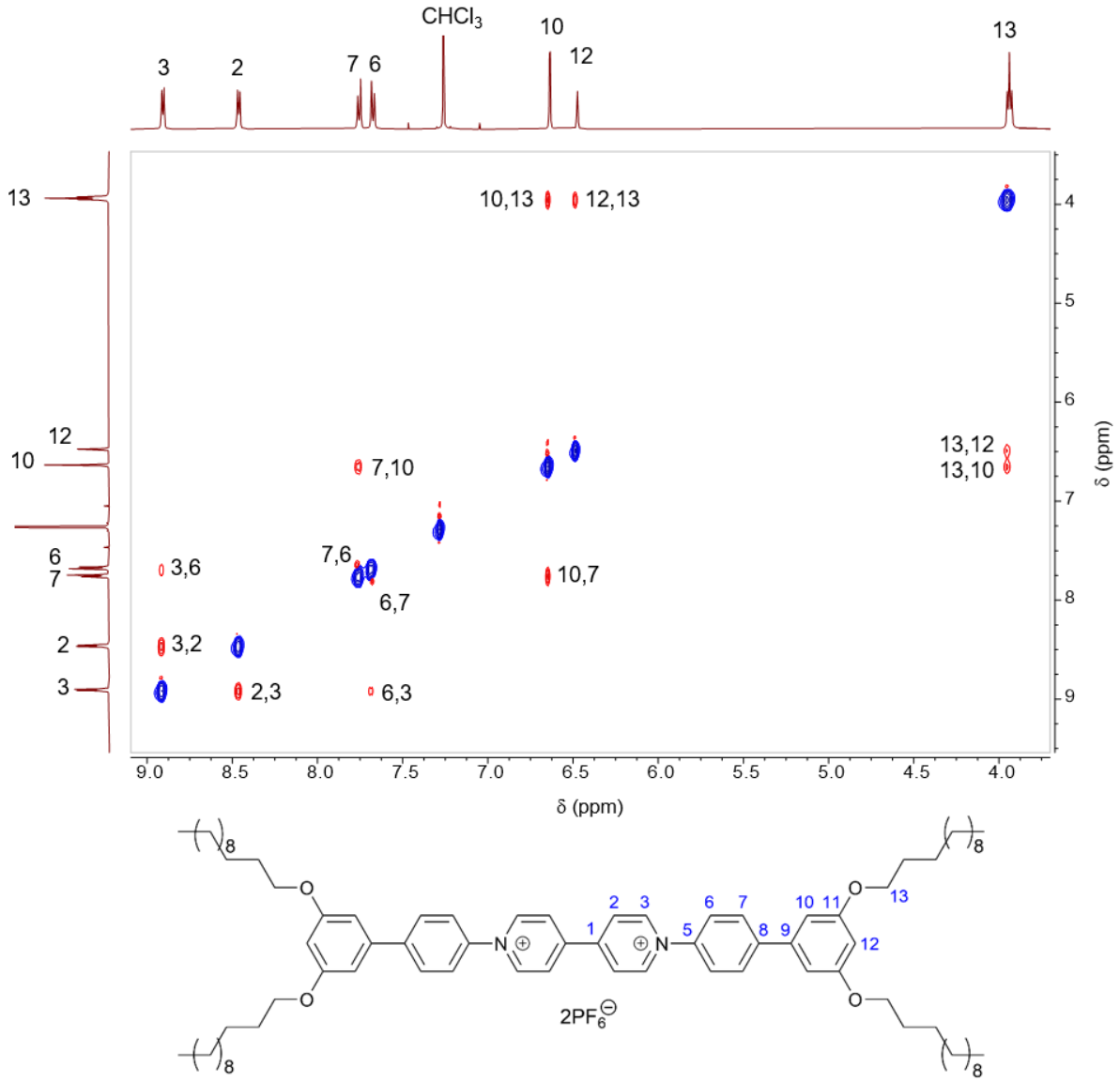

Figure S16. ROESY NMR spectrum (500 MHz, $CDCl_3$) of viologen **ArV-C12**.

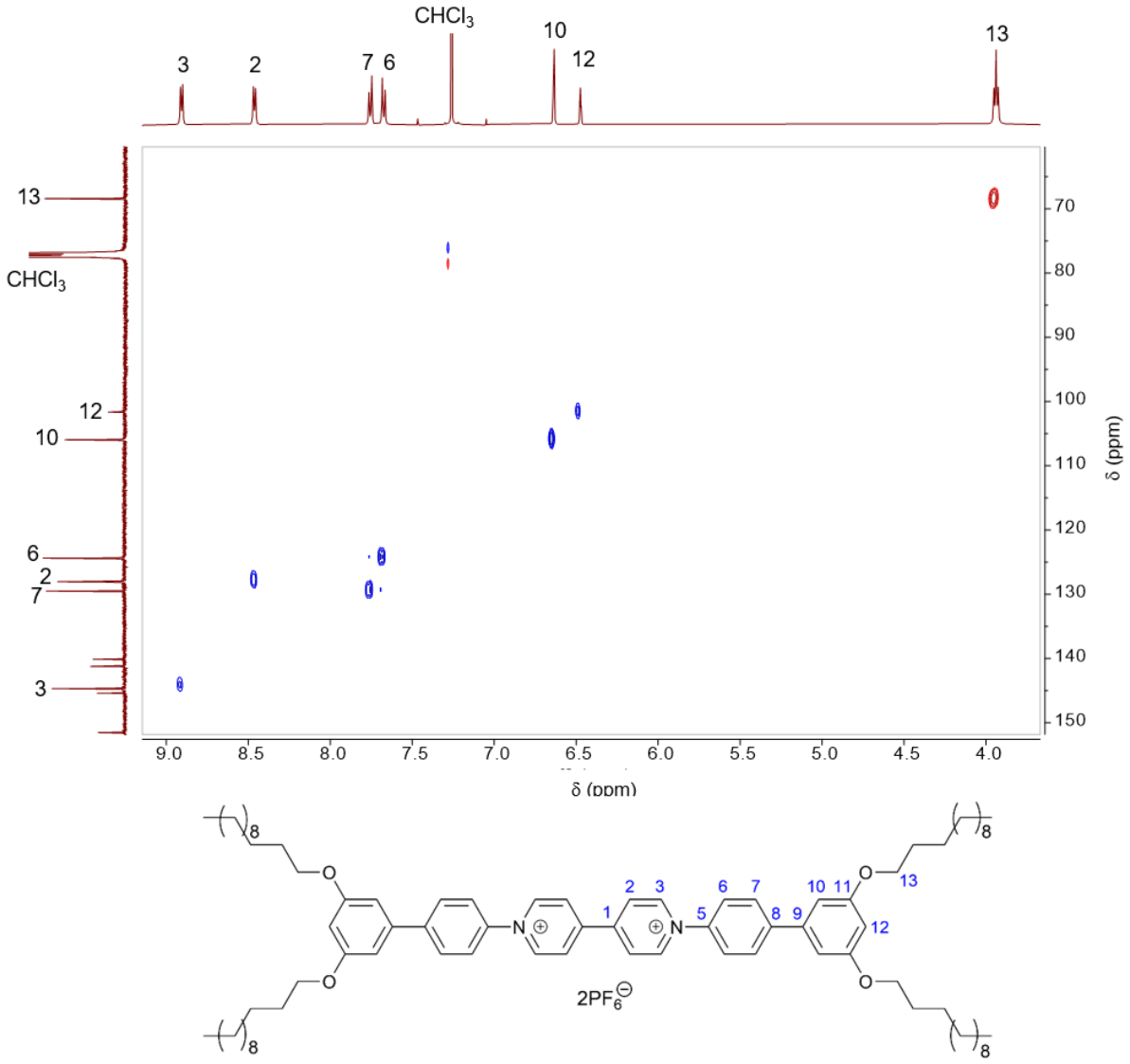

Figure S17. ^{1}H-^{13}C HSQC NMR spectrum (500 MHz, $CDCl_3$) of viologen **ArV-C12**.

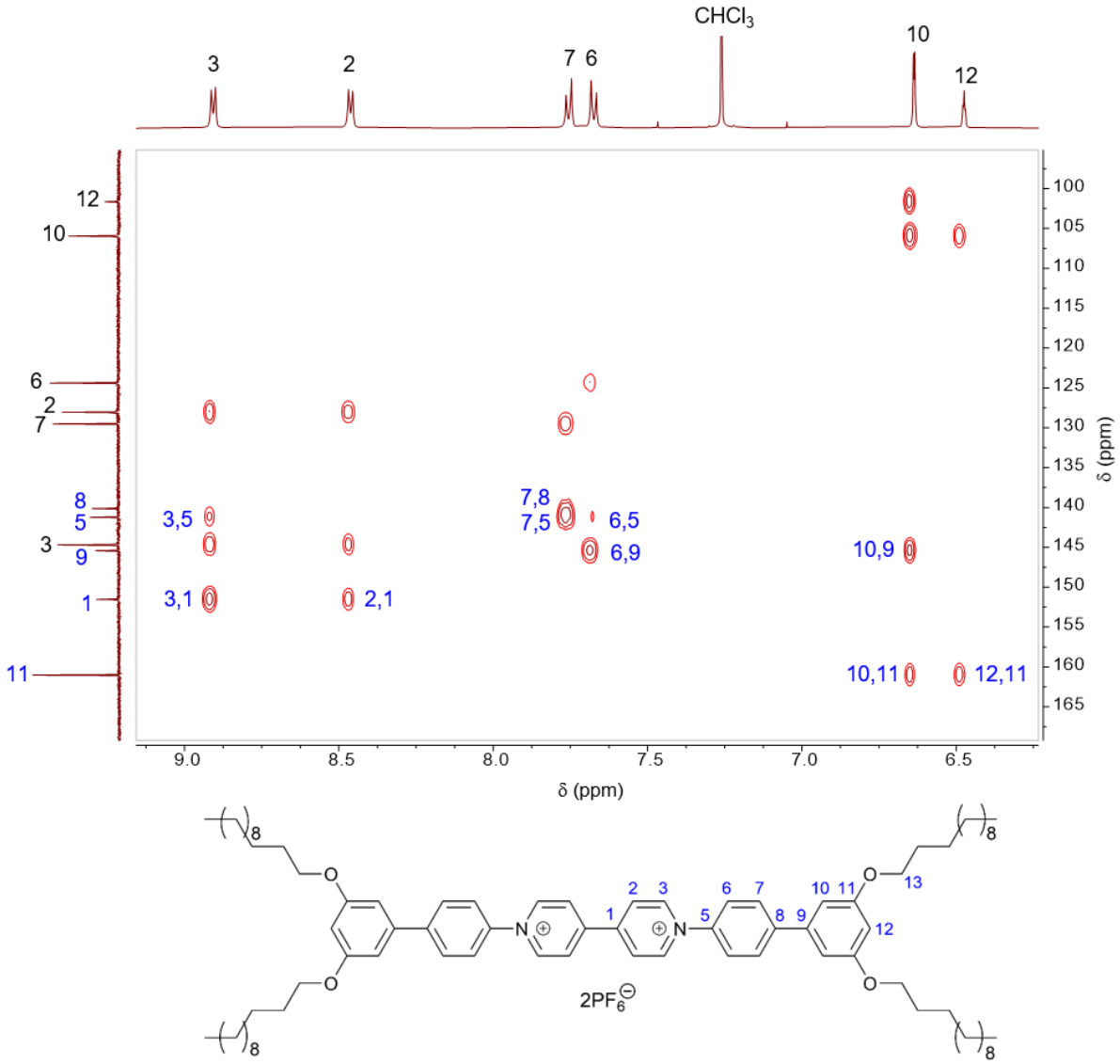

Figure S18. ^{1}H-^{13}C HMBC NMR spectrum (500 MHz, $CDCl_3$) of viologen **ArV-C12**. Attributions in blue were determined with this spectrum.

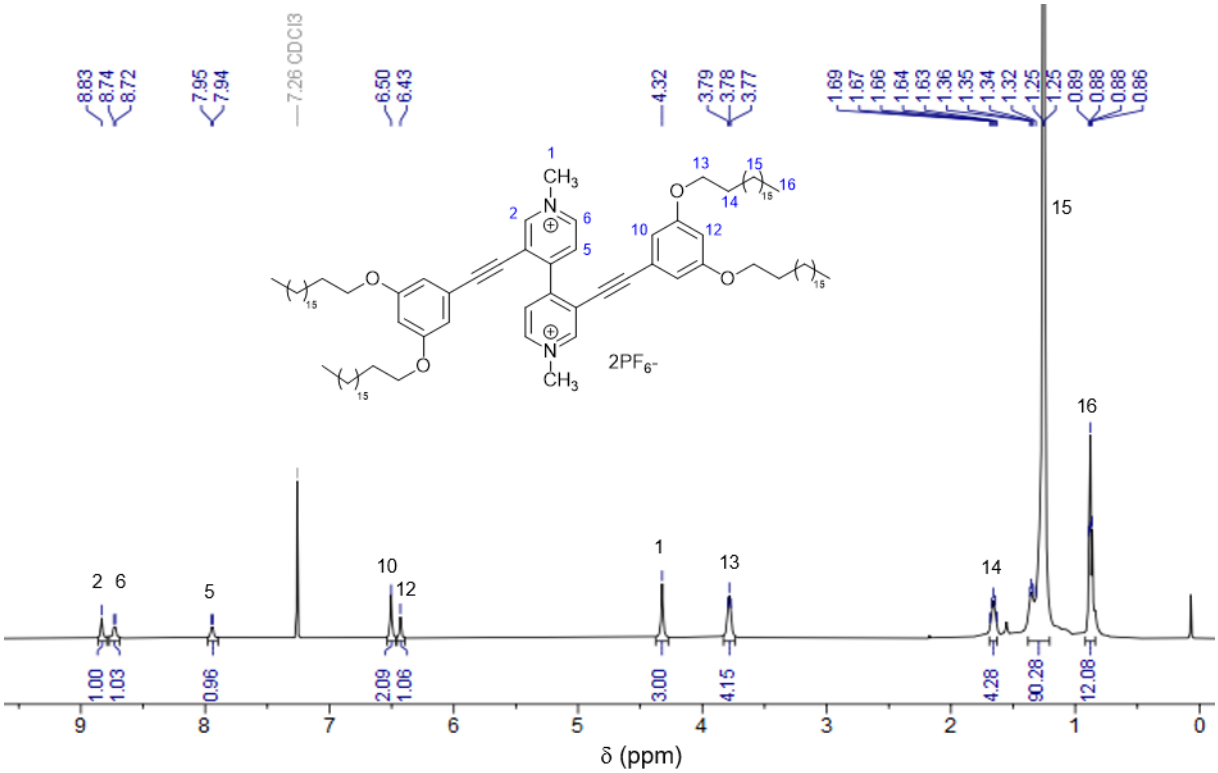

Figure S19. ^{1}H NMR (400 MHz, $CDCl_3$) of viologen **MV-C18**.

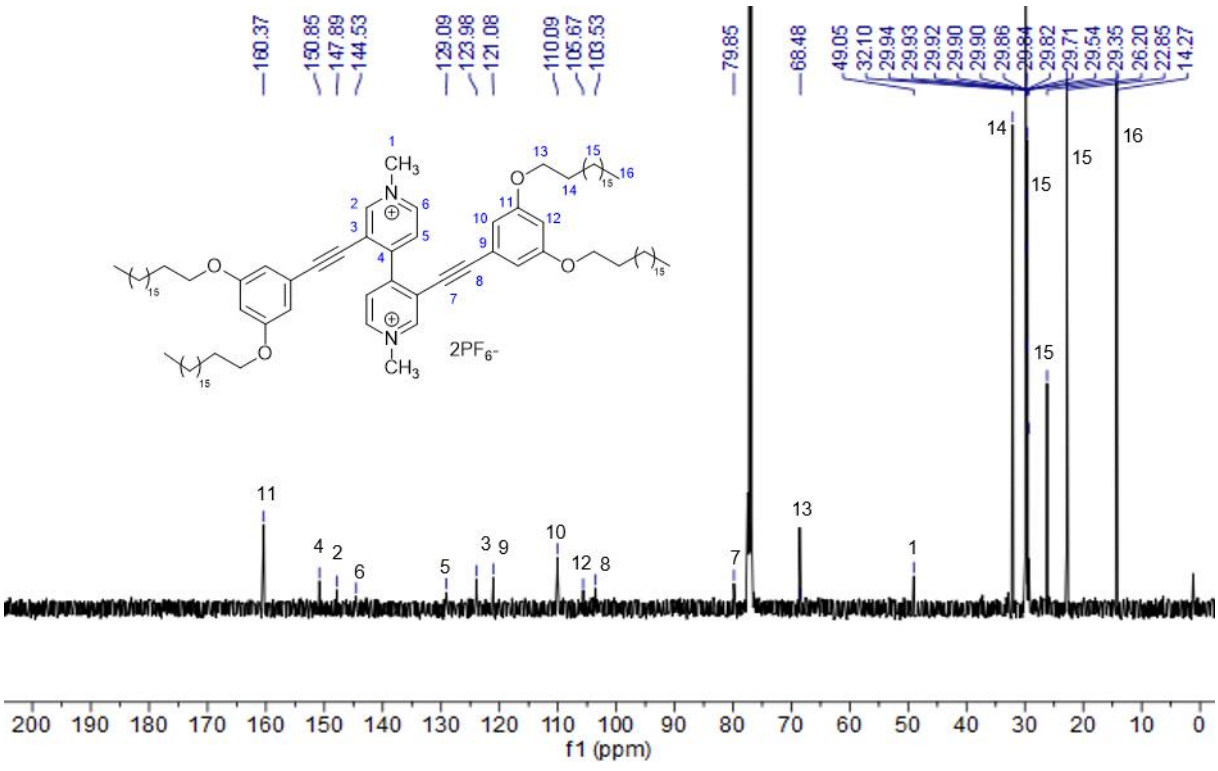

Figure S20. ^{13}C NMR (125 MHz, $CDCl_3$) of viologen **MV-C18**.

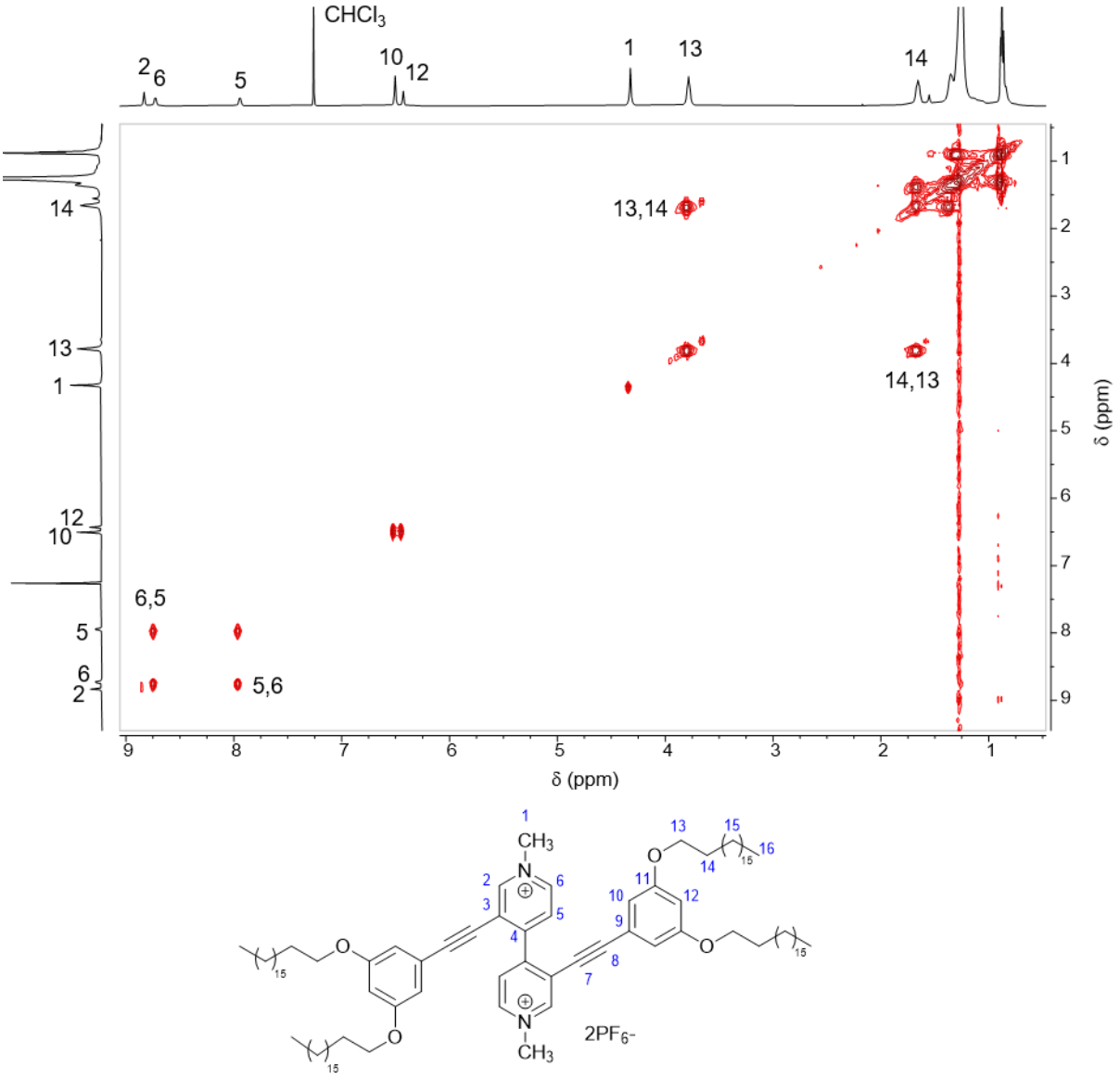

Figure S21. COSY NMR (500 MHz, $CDCl_3$) of viologen **MV-C18**.

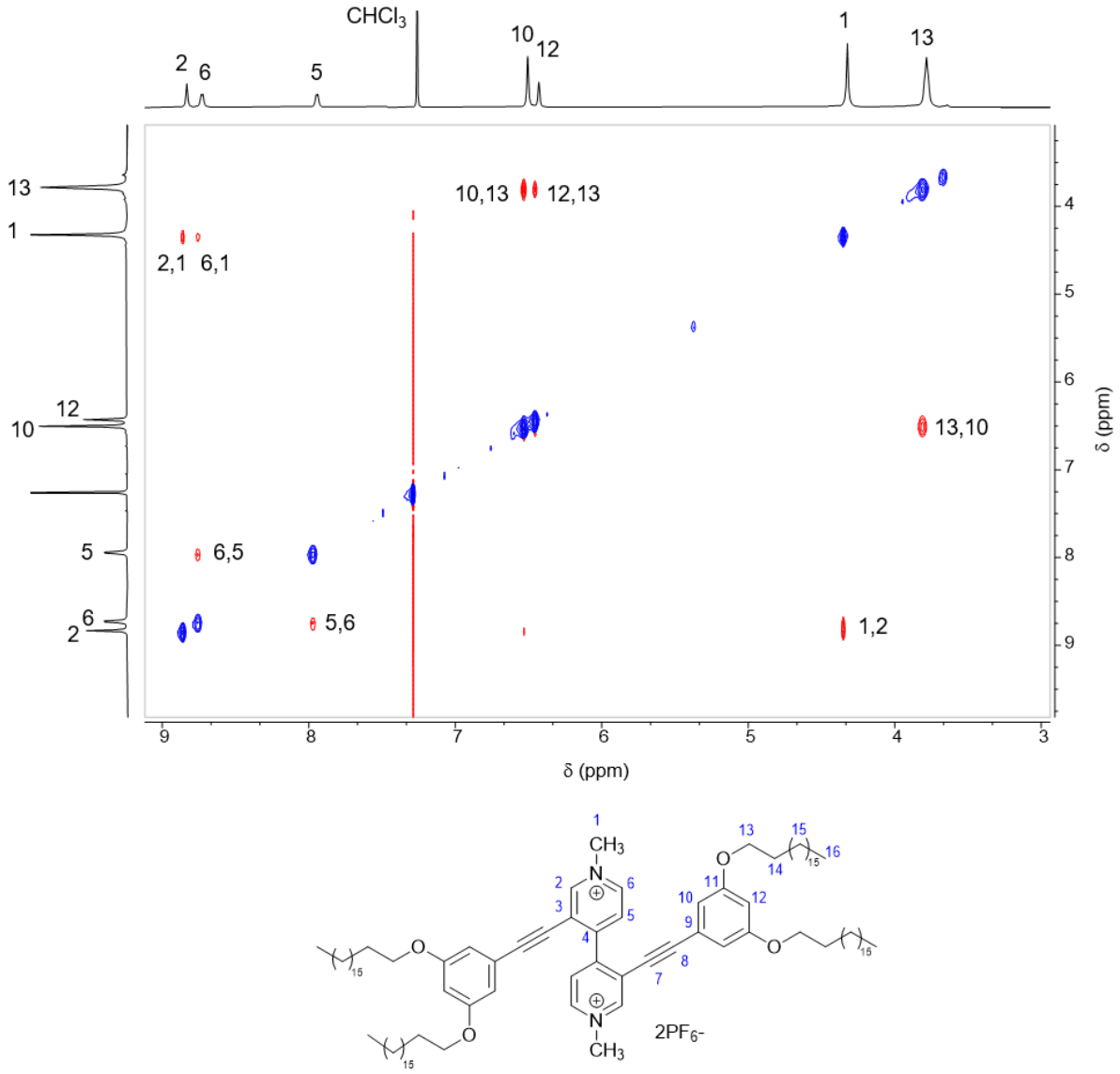

Figure S22. ROESY NMR (500 MHz, $CDCl_3$) of viologen **MV-C18**.

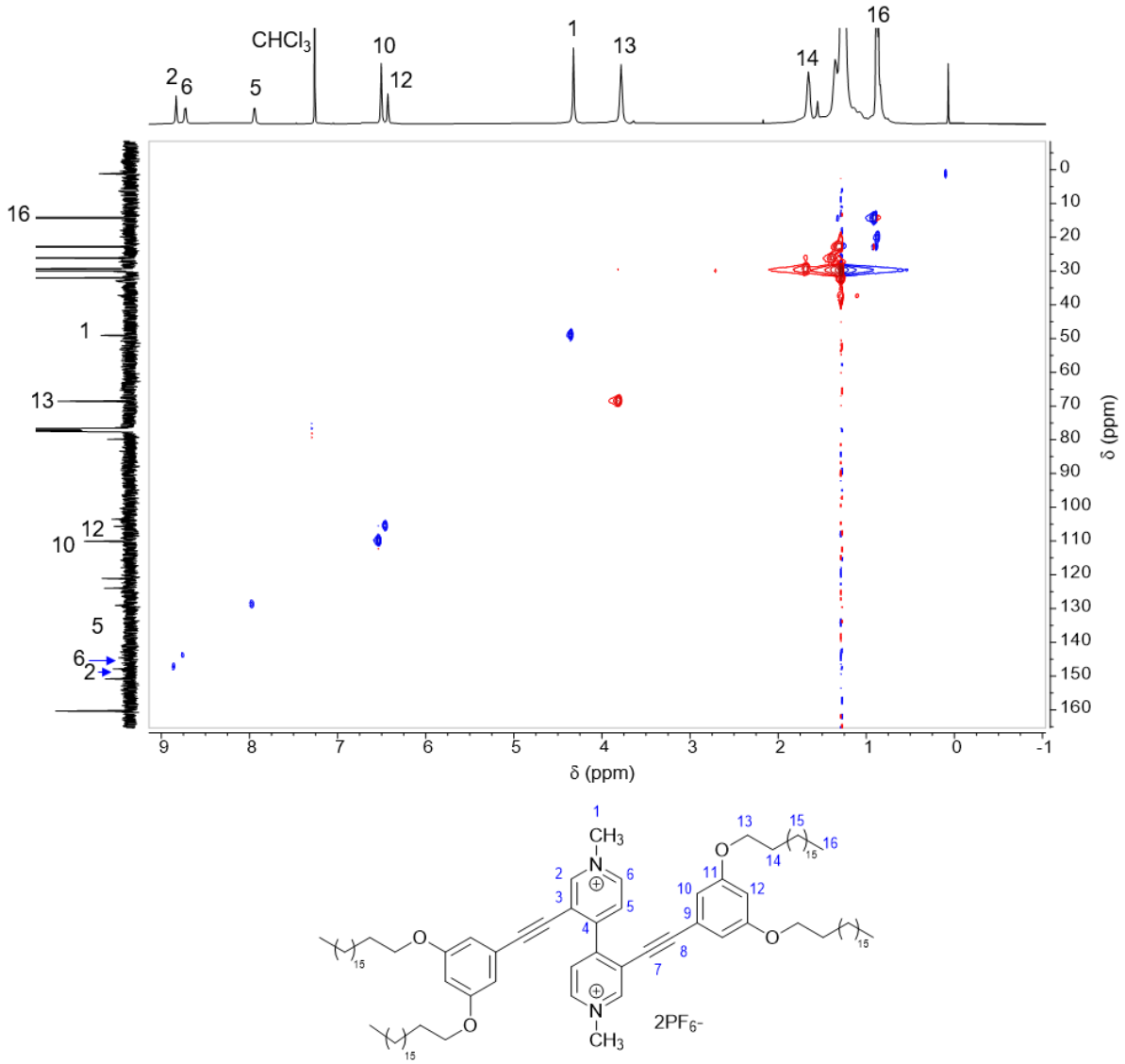

Figure S23. ^{1}H-^{13}C HSQC NMR (500 MHz, $CDCl_3$) of viologen **MV-C18**.

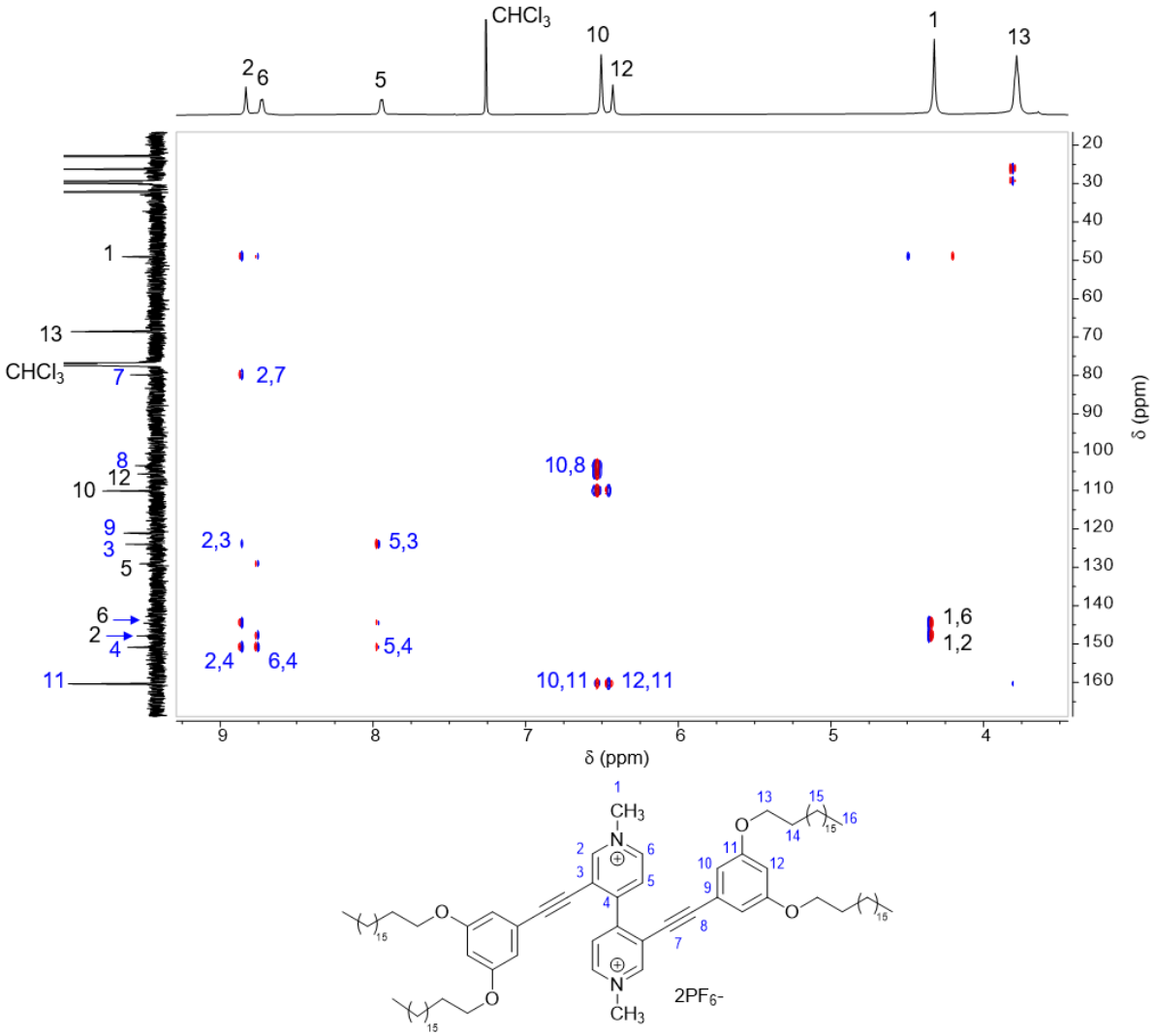

Figure S24. ^{1}H-^{13}C HMBC NMR (500 MHz, $CDCl_3$) of viologen **MV-C18**. Attributions in blue were determined with this spectrum.

Table S1. ^{1}H and ^{13}C Chemical shifts of viologens **ArV-C8** in $CDCl_3$.

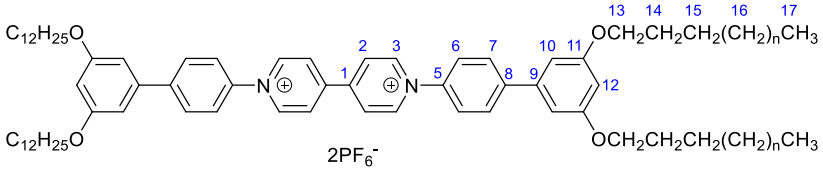

ArV-C8: n = 4

ArV-C8	**solution**		**Solid state**	
position	**δ ^{1}H** (ppm)	**δ ^{13}C** (ppm)	**δ ^{1}H** (ppm)	**δ ^{13}C** (ppm)
1		151.5		148.7
2	8.45	128.1	8.7	124.9
3	8.90	144.7	8.6	142.7
4	-	-	-	-
5	-	141.2	-	140.18
6	7.67	124.4	7.8	123.51
7	7.74	129.5	7.7	127.71
8	-	140.1	-	142.23
9	-	145.4	-	140.34
10	6.63	106.0	7.2	108.98
10’	-	-	7.1	102.48
11	-	161.0	-	159.59
12	6.47	101.6	7.1	100.39
13	3.93	68.4	4.4	67.04
13’	-	-	3.9	66.18
14	1.77	29.6	1.4	31.13
15	1.43	26.2	1.9	30.29
16	1.28-1.33	32.0, 29.43, 29.42, 22.8,	1.7, 0.8, 1.9, 1.7	29.56, 28.53, 26.48, 22.88
17	0.88	14.3	1.6	13.89

Table S2. ^{1}H and ^{13}C Chemical shifts of viologens **ArV-C12** in $CDCl_3$.

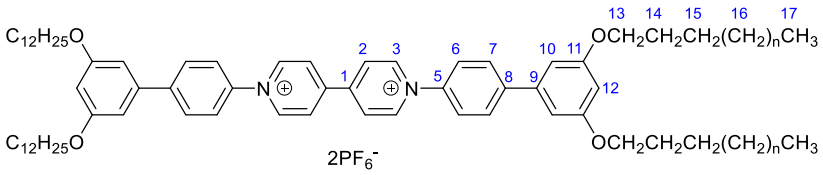

ArV-C12: n = 8

ArV-C12				
	solution		Solid state	
position	**δ ^{1}H** (ppm)	**δ ^{13}C** (ppm)	**δ ^{1}H** (ppm)	**δ ^{13}C** (ppm)
1		151.5		149.01
2	8.46	128.1	8.7	126.02
3	8.90	144.7	8.7	143.83
4	-		-	-
5	-	141.2	-	141.30
6	7.68	124.4	8.0	124.75
7	7.75	129.5	7.8	128.5
8	-	140.1	-	143.26
9	-	145.4	-	141.69
10	6.63	105.9	7.4	109.28
10’			7.2	104.45
11	-	161.0	-	160.41
12	6.47	101.6	7.4	101.42
13	3.93	68.4	4.7	67.69
14	1.77	29.46	2.3	33.38
15	1.45	26.2	2.32	31.20
16	1.26-1.33	32.1, 29.9, 29.82, 29.79	1.37, 2.41, 0.84, 2.28,	30.72, 27.25, 26.62, 23.58
17	0.88	14.3	1.8	14.47

Table S3. ^{1}H and ^{13}C Chemical shifts of viologen **MV-C18** in $CDCl_3$.

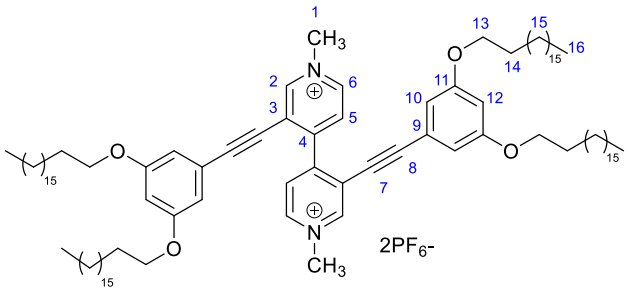

MV-C18				
	solution		Solid state	
position	**δ ^{1}H** (ppm)	**δ ^{13}C** (ppm)	**δ ^{1}H** (ppm)	**δ ^{13}C** (ppm)
1	4.32	49.1	4.2	48.32
2	8.83	147.9	8.6	148.5 <-> 146.6
3	-	124.0	-	122.98
4	-	150.9	-	145.65
5	7.94	129.1	7.9	128.10
6	8.73	144.5	9.1	145.7 <-> 142.7
7	-	79.9	-	-
8	-	103.5	-	-
9	-	121.1	-	121.18
10	6.50	110.1	6.8	110.1 <-> 106.7
11	-	160.4	-	159.8
12	6.43	105.7	6.3	105.3 <-> 101.7
13	3.78	68.5	3.9	68.34
14	1.67	29.35	1.1	25.91
15	1.48-1.10	29.9-22.8	1.2	29.63
16	0.88	14.3	1.5	22.61

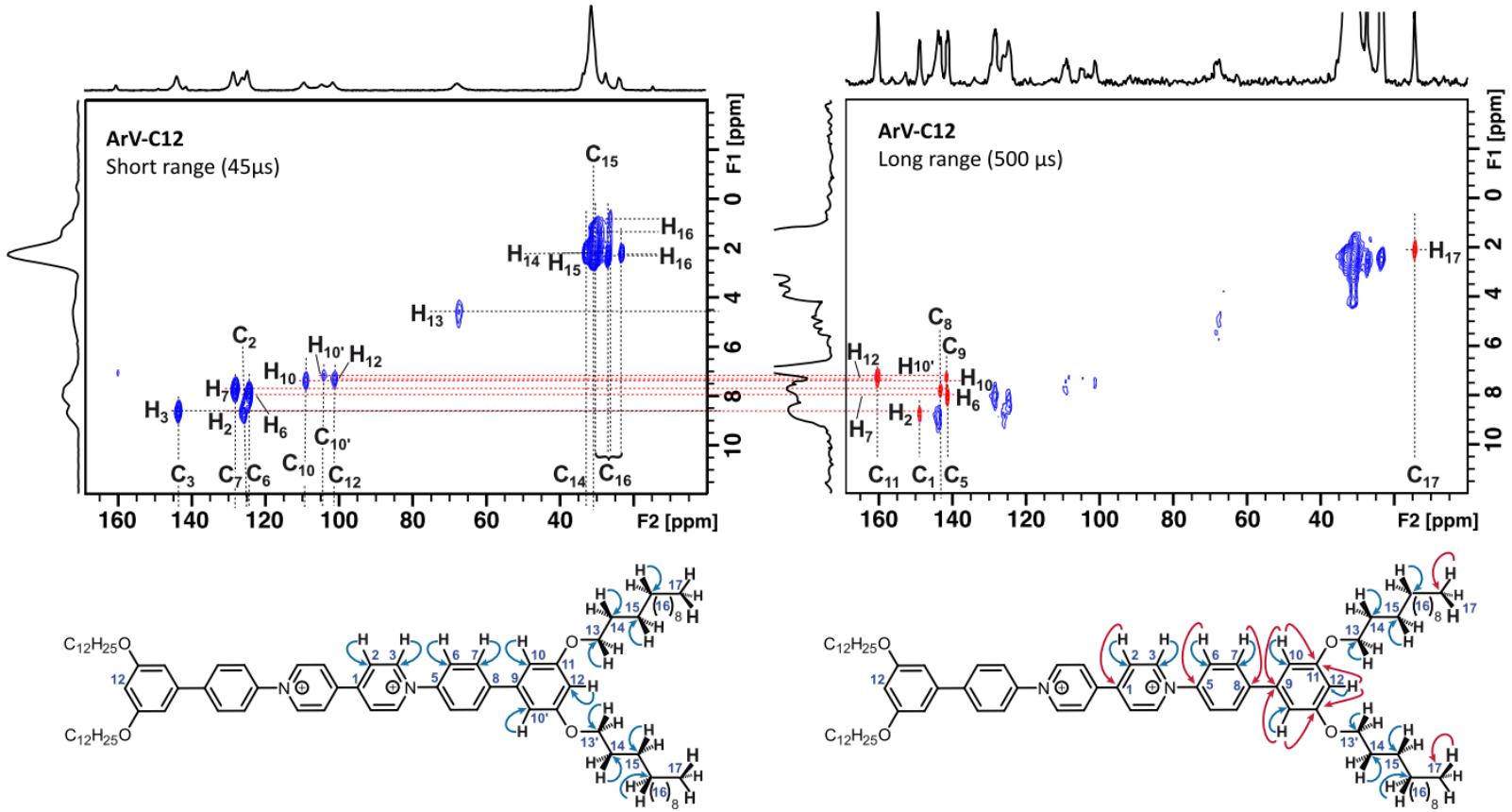

Figure S25. ^{1}H-^{13}C HETCOR of **ArV-C12** with FSLG irradiation during the evolution time with short contact time (45 µs, top left map) and long contact time (500 µs, top right map). At 45 µs contact time only protons directly attached to their carbon will be significantly polarized, except for the methyls for which the fast rotation along the CH_3 axis partly averages the dipolar coupling. Nevertheless, the top trace shows that even the quaternary carbons are slightly polarized; however, their weak intensities allow easy differentiation from CH_2s and CHs. The polarization pathways are indicated as blue arrows in the bottom left drawing. The CH_2s and CHs are readily assigned from the correlation map analysis. Quaternary carbons and methyls appear when time enough remains to allow proper buildup of coherences for smaller dipolar couplings, as is the case for quaternary carbon and methyls (top right map): quaternaries because they are further from protons and methyls because the fast rotation around their axis partly averages the dipolar constant. In comparison with the short-range correlations, some new peaks appear (colored in red) in the long-range correlations. The origin of the latter is depicted in the lower right molecular scheme with red arrows for polarization pathways. The 1 ms contact time map then allows assignment for the quaternary carbons and the methyl as shown. This correlation map is obtained for the supramolecular assembly, not the viologen alone, and conversely the PF_6^- anion plays a role by adding a small asymmetry; carbons 10 and 10' as well as protons 10 and 10' differ due to their variable distance from PF_6^- in the 3D construct (see Figure 3).

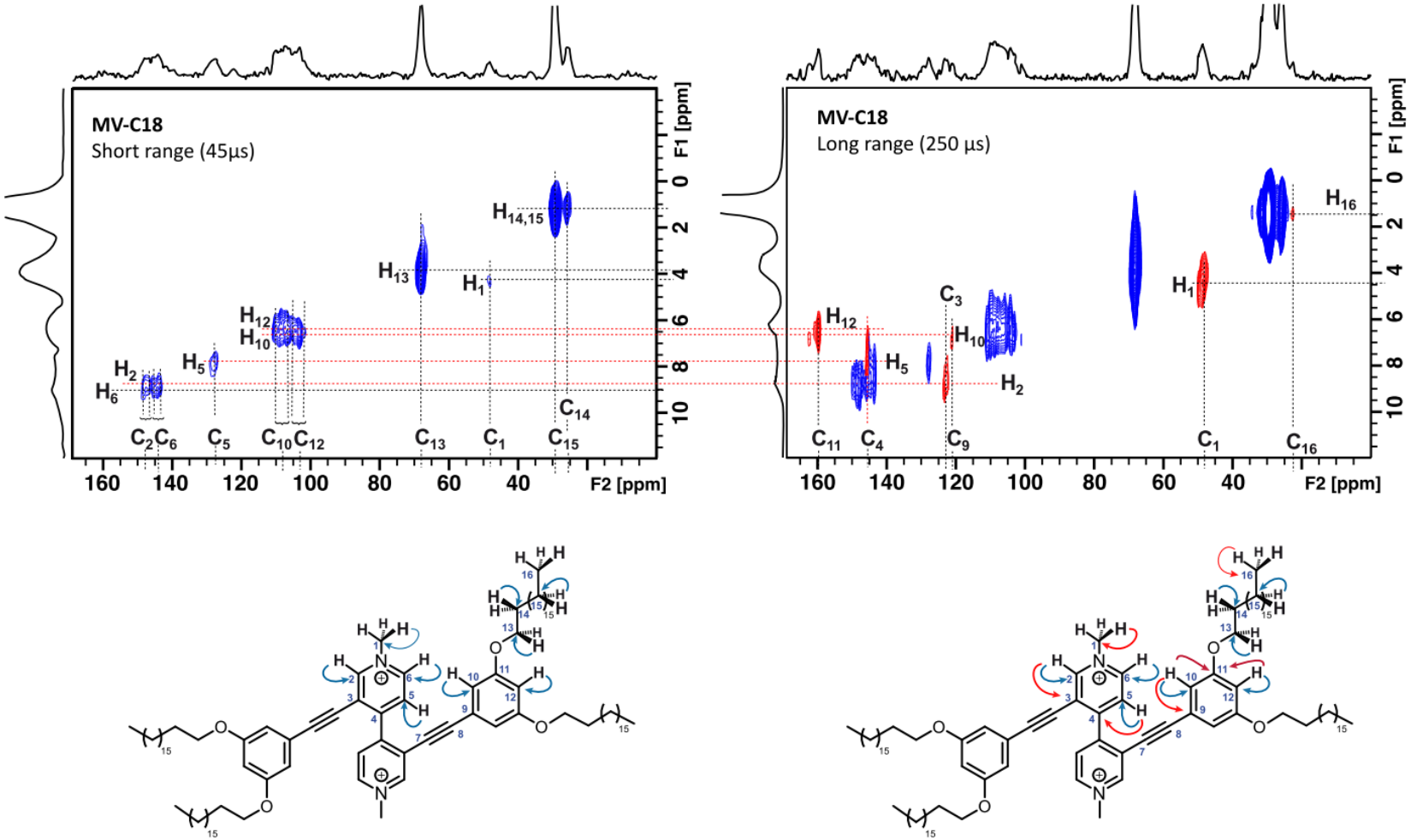

Figure S26. ^{1}H-^{13}C HETCOR of **MV-C18,** with FSLG irradiation during the evolution time. Top left spectrum for short contact time (45 µs, blue arrows for polarization pathways in bottom left drawing) and top right map for long contact time (250 µs, red arrows for more remote polarization pathways in bottom right drawing). The signals of **MV-C18** are assigned in the same way as for **ArV-C12** as explained in Figure S25. However, because of the dozen or so structures present in this case, carbons 2, 3, 6, 10 and 12 as well as protons 2, 6, 10 and 12 show a small dispersion in chemical shift and appear in poorly resolved clusters. Nevertheless, by comparison with the long-distance experiment (top right), it becomes possible to distinguish the protons. The same is not obvious with the carbons, but by analogy with the liquid-state NMR spectra it is still possible to group them as described in the map at top left. Note that with the employed parameters carbons 8 and 9 are at noise level and not detected.

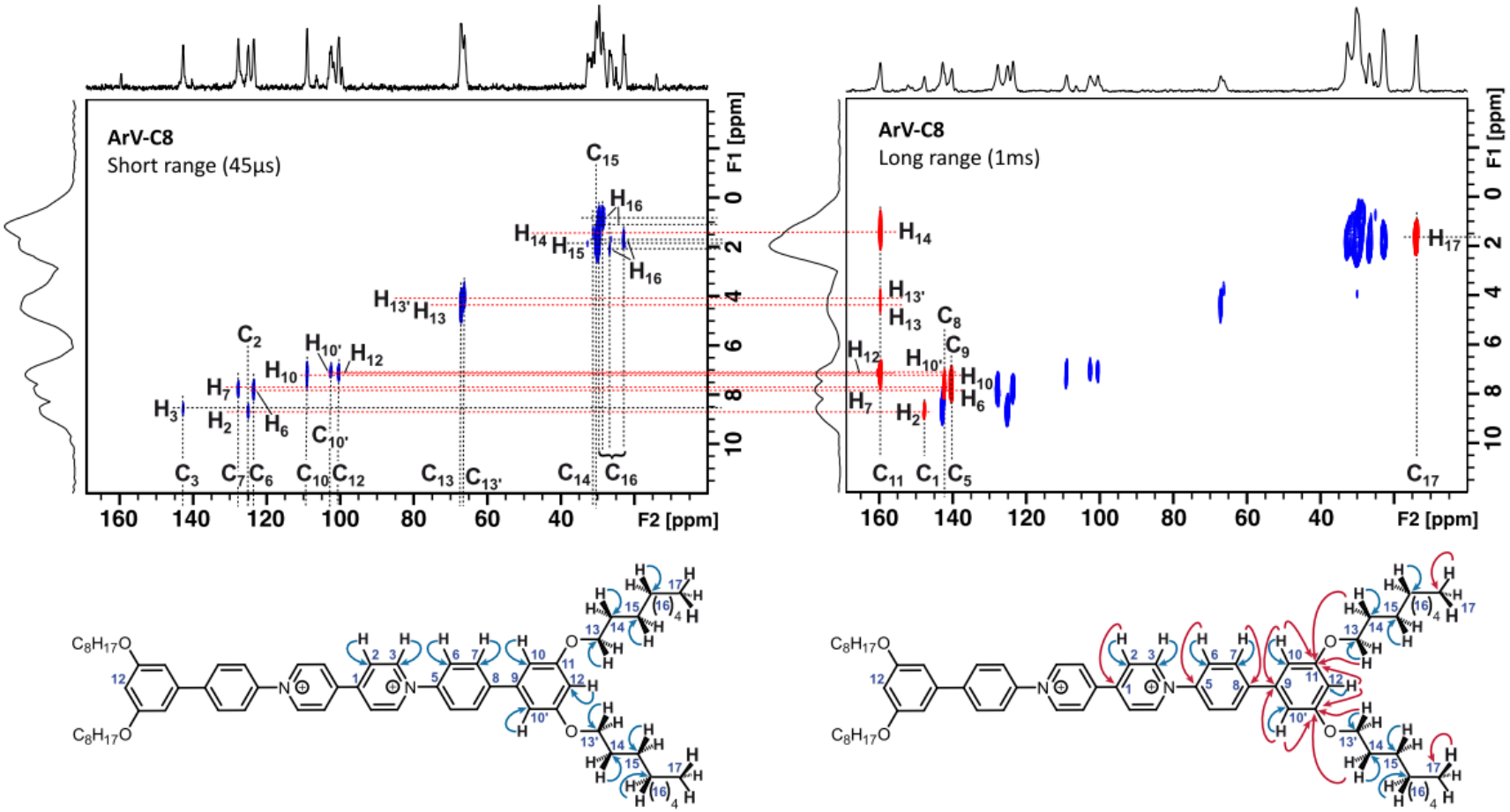

Figure S27. ^{1}H-^{13}C HETCOR of **ArV-C8**, with FSLG irradiation during the evolution time. Top left spectrum for short contact time (45 µs, blue arrows for polarization pathways in bottom left drawing) and top right map for long contact time (1 ms, red arrows for more remote polarization pathways in bottom right drawing). The signals of are assigned in the same way as for **ArV-C12** as explained in Figure S25. Here again, the variable distance from the PF_6^- anion in the 3D construct leads to a differentiation of positions 10 and 13 into 10, 10', 13 and 13'.

Figure S28. Topography AFM images (2.15 x 2.15 μm^2) of a HOPG surface after the drop casting of pure $CHCl_3$.

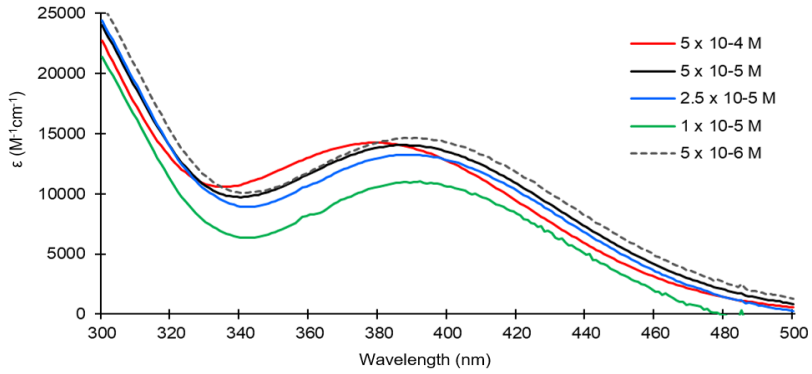

concentration	λ (nm)
5×10^{-4}	378
5×10^{-5}	387
2.5×10^{-5}	390
1×10^{-5}	392
5×10^{-6}	392

Figure S29. UV-visible spectra and wavelengths of the lowest energy absorption band of **ArV-C8** at various concentrations in $CHCl_3$.

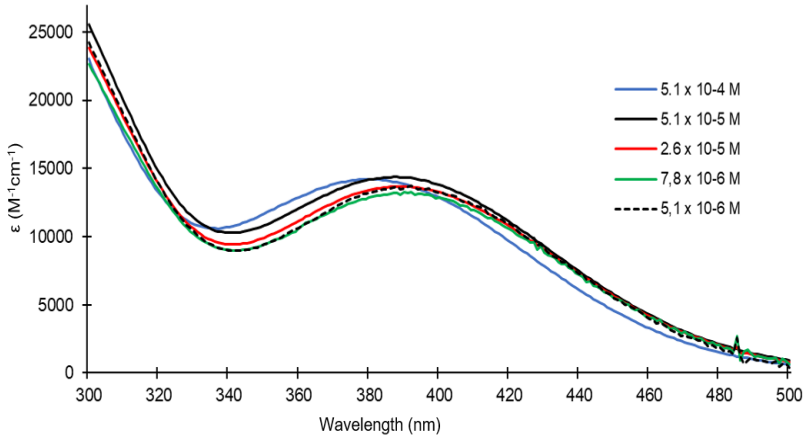

concentration	λ (nm)
5.1×10^{-4}	381
5.1×10^{-5}	387
2.6×10^{-5}	388
7.8×10^{-6}	392
5.1×10^{-6}	392

Figure S30. UV-visible spectra and wavelengths of the lowest energy absorption band of **ArV-C12** at various concentrations in $CHCl_3$.

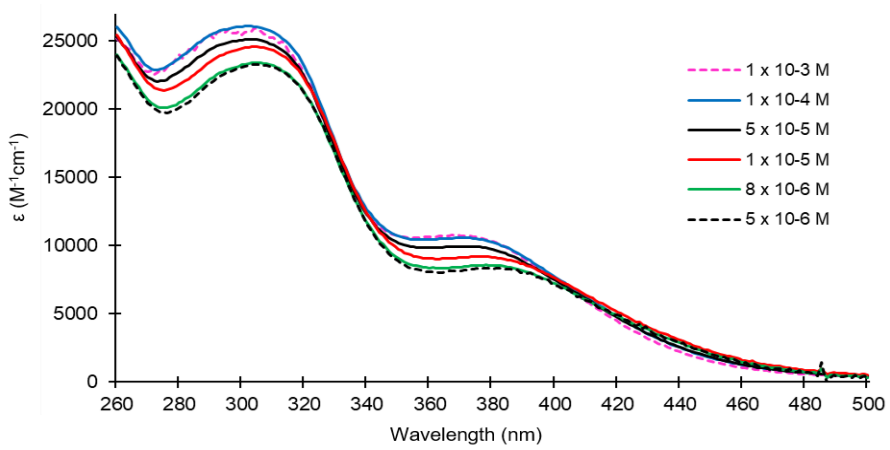

concentration	λ (nm)
1×10^{-3}	369
1×10^{-4}	371
5×10^{-5}	372
1×10^{-5}	377
8×10^{-6}	378
5×10^{-6}	378

Figure S31. UV-visible spectra and wavelengths of the lowest energy absorption band of **MV-C18** at various concentrations in $CHCl_3$.

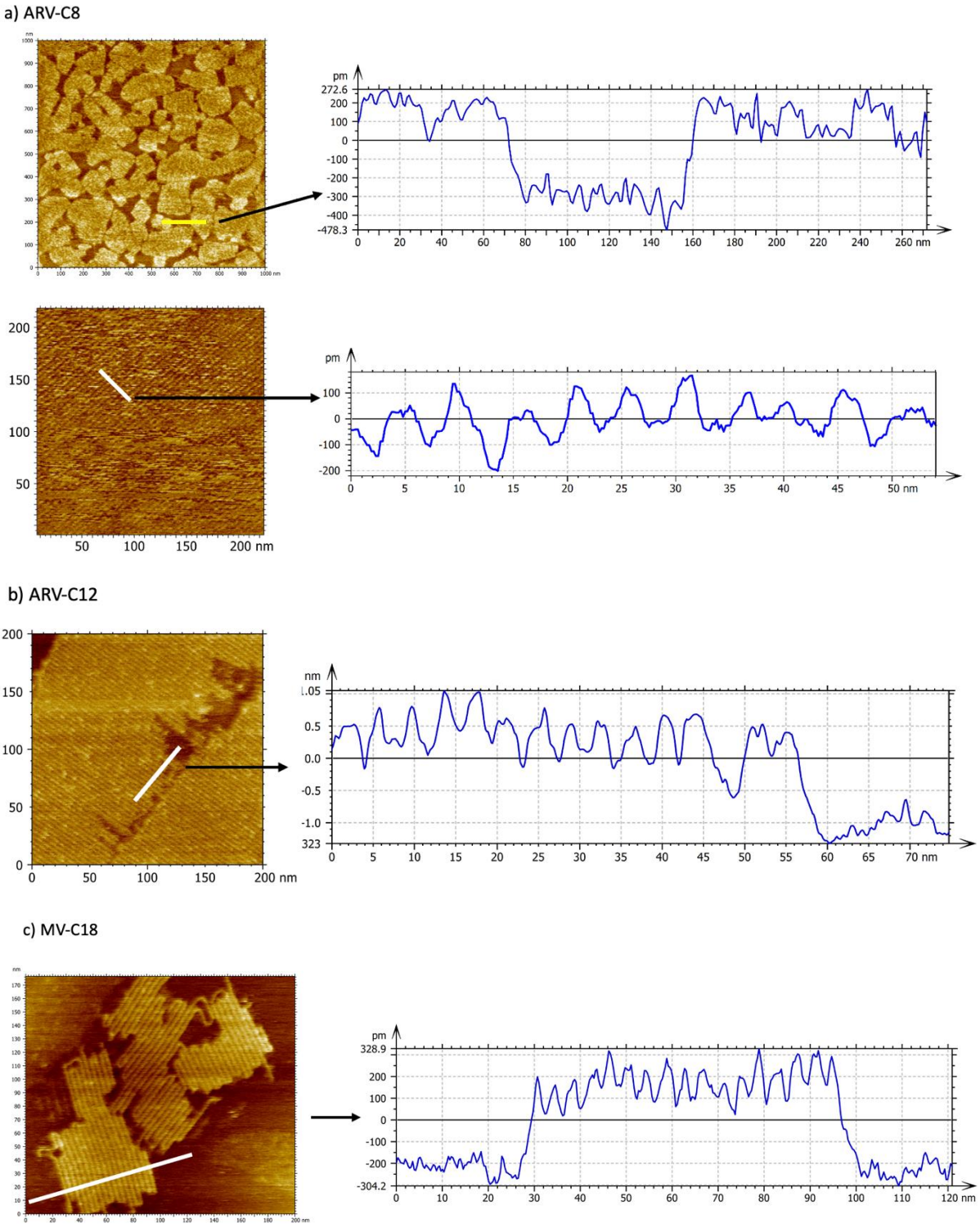

Figure S32. Z-profiles taken along the white (periodicity) or yellow (height) line from the topography AFM images on an HOPG surface after the deposition of a) **ArV-C8** (1000 x 1000 nm^2, and 250 x 250 nm^2), b) **ArV-C12** (200 x 200 nm^2) and c) **MV-C18** (150 x 150 nm^2). The periodicities between adjacent bright nanolines are 4.51 nm, 4.14 nm and 4.00 nm respectively.

a)

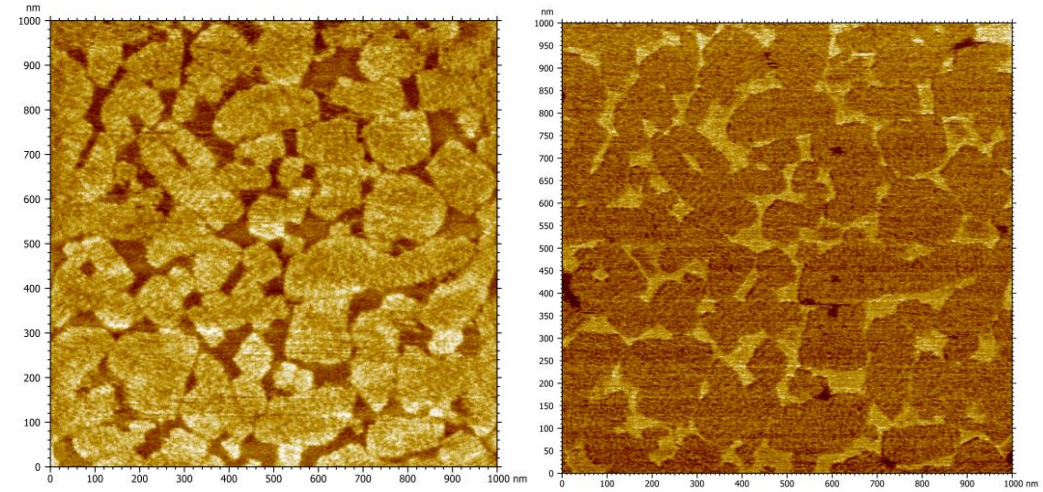

b)

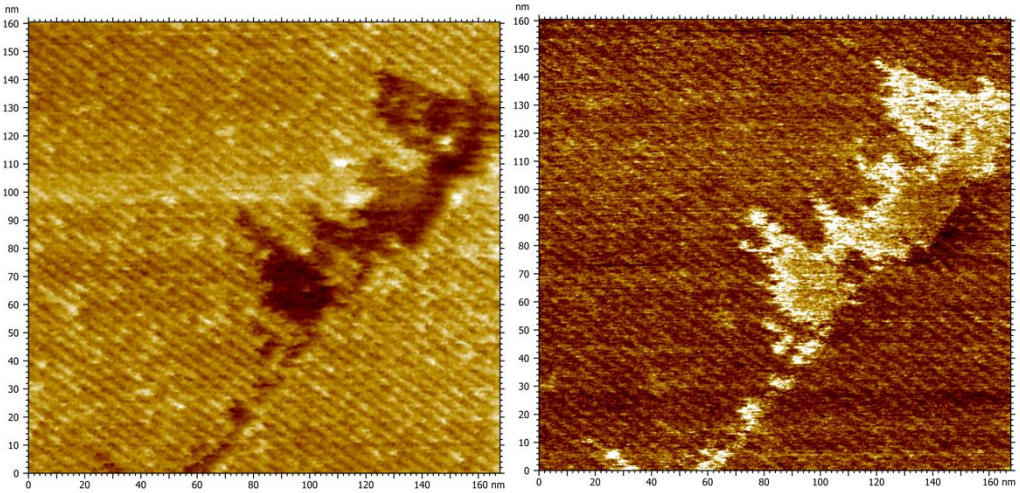

c)

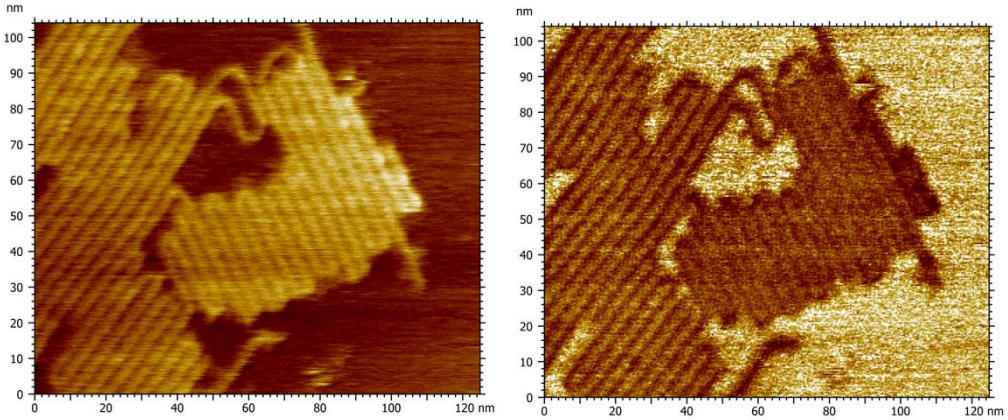

Figure S33. Topography (left) and corresponding adhesion (right) AFM images on an HOPG surface after the deposition of a) **ARV-C8** (1000 x 1000 nm^2), b) **ARV-C12** (165 x 165 nm^2) and c) **MV-C18** (125 x 125 nm^2). A comparison of adhesion images between areas attributed to the supramolecular network and other areas reveals significantly different adhesion signals. This difference strongly indicates that there is no supramolecular network in the uncovered areas.

a) ARV-C8

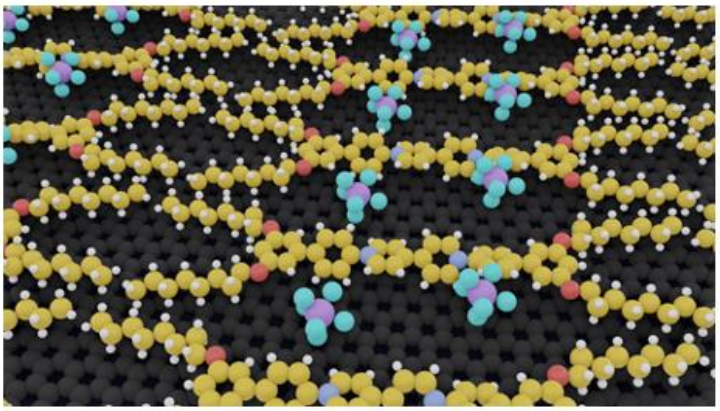

b) ARV-C12

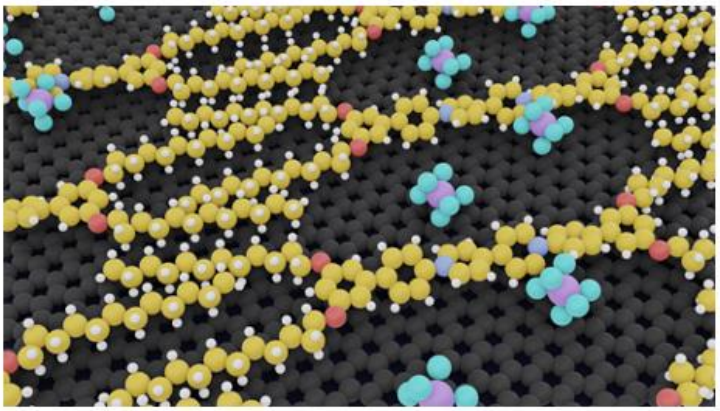

c) MV-C18

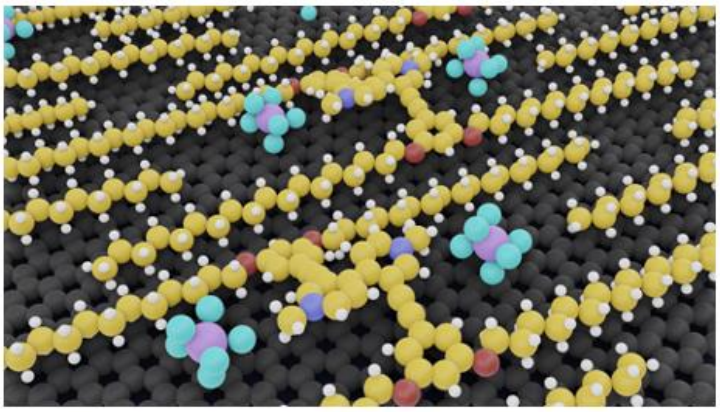

Figure S34. Side-view of adsorption models of supramolecular networks on a HOPG surface based on a) **ArV-C8**, b) **ArV-C12** and c) **MV-C18** organic salts. The position of hexafluorophosphate anions has been determined thanks to solid-state NMR experiments.